Antivirulence C-Mannosides as Antibiotic-Sparing, Oral Therapeutics for Urinary Tract Infections

Laurel Mydock-McGrane,[†,#] Zachary Cusumano,[†,#] Zhenfu Han,[‡] Jana Binkley,[§] Maria Kostakioti,[§] Thomas Hannan,[†] Jerome S. Pinkner,[§] Roger Klein,[§] Vasilios Kalas,[§] Jan Crowley,[∥] Nigam P. Rath,[⊥] Scott J. Hultgren,[†,§,∥] and James W. Janetka*,[†,‡,∥]

[†]Fimbrion Therapeutics, Inc., Saint Louis, Missouri 63108 United States

[‡]Departments of Biochemistry and Molecular Biophysics, and Chemistry, [§]Department of Molecular Microbiology, [∥]Center for Women's Infectious Disease Research, Washington University School of Medicine, Saint Louis, Missouri 63110 United States

[⊥]Department of Chemistry and Biochemistry, University of Missouri, Saint Louis, Missouri 63121 United States

ⓢ *Supporting Information*

ABSTRACT: Gram-negative uropathogenic *Escherichia coli* (UPEC) bacteria are a causative pathogen of urinary tract infections (UTIs). Previously developed antivirulence inhibitors of the type 1 pilus adhesin, FimH, demonstrated oral activity in animal models of UTI but were found to have limited compound exposure due to the metabolic instability of the *O*-glycosidic bond (*O*-mannosides). Herein, we disclose that compounds having the *O*-glycosidic bond replaced with carbon linkages had improved stability and inhibitory activity against FimH. We report on the design, synthesis, and in vivo evaluation of this promising new class of carbon-linked *C*-mannosides that show improved pharmacokinetic (PK) properties relative to *O*-mannosides. Interestingly, we found that FimH binding is stereospecifically modulated by hydroxyl substitution on the methylene linker, where the *R*-hydroxy isomer has a 60-fold increase in potency. This new class of *C*-mannoside antagonists have significantly increased compound exposure and, as a result, enhanced efficacy in mouse models of acute and chronic UTI.
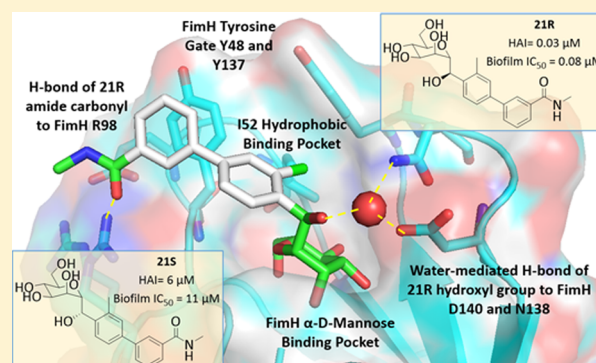
INTRODUCTION

Since the 1970s, antibiotic resistance has been steadily increasing and now multidrug resistant pathogens are an imminent threat. Antibiotics target processes essential for bacterial replication and thus induce strong pressure to evolve resistance to these drugs. An alternate therapeutic strategy is to disarm the pathogen by inhibiting critical host−pathogen interactions necessary for persistence in a host. Herein, we describe a promising antibiotic-sparing strategy using small molecule *C*-mannosides that specifically block the ability of uropathogenic *Escherichia coli* (UPEC) to colonize the lower urinary tract by neutralizing the FimH adhesin. In mouse models, we show that *C*-mannosides are oral drugs that are effective in both preventing and treating urinary tract infections (UTIs). These compounds represent advanced preclinical candidates for UTI therapy.

Microbial adherence to host cells is a critical initial step in most infectious diseases.[1] The ability of bacteria to bind and invade epithelial tissues allows them to establish a niche within the host and evade host immune responses.[2] While antimicrobial therapy has traditionally been effective in treating bacterial infections, resistance to the most commonly used antimicrobials is on the rise,[3] highlighting the need for new

therapeutic strategies.[4] The study of critical host−pathogen interactions during bacterial infection has revealed promising novel targets for therapeutic intervention.[5] Monoclonal antibodies, vaccines, glycoconjugates, and small molecules have all been developed to disrupt bacterial adherence by competitively blocking the bacterial protein(s) involved in the recognition of various host receptors.[6] This process and molecular mechanism has been most thoroughly studied in urinary tract infection (UTI) pathogenesis.

A key step in UTI pathogenesis is the initial colonization of the bladder epithelium by uropathogenic *E. coli* (UPEC). This binding is mediated by hair-like fibers, termed type 1 pili, that are tipped with the virulence factor FimH adhesin.[7] The lectin domain of FimH binds mannosylated glycoproteins expressed on the luminal surface of human and murine bladder cells. The terminal FimH residue is a prototypical two-domain adhesin, which is joined to the distal end of the linear tip fibrillum of type 1 pili by a donor strand exchange reaction with subunit FimG.[7,8] FimG then undergoes its own donor strand exchange reaction with subunit FimF, which adapts the fibrillum tip to
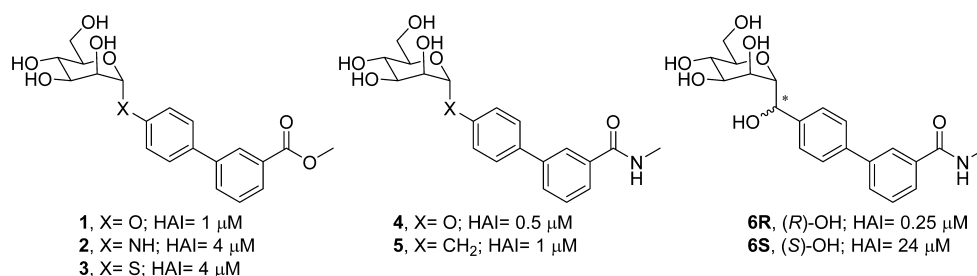
Figure 1. Examples of simple glycosidic bond replacement of early lead O-mannosides **1** and **4**, with alternate linkers to the biphenyl aglycone.

the long pilus rod, which consists of a homopolymer of ~1000 FimA subunits coiled into a rigid right-handed helical structure that is capable of unwinding into a linear fiber.[9] The FimH lectin domain contains a deep acidic pocket that recognizes α-D-mannose with stereochemical specificity.[8] FimH-mediated binding to mannosylated uroplakins[10] or α1,β3 integrins[11] facilitates bacterial colonization and invasion of bladder epithelial cells.[12]

UTIs present a significant burden for women, with nearly 20 million cases reported annually.[13] Despite antibiotic treatment, 20−40% of these women will have at least one recurrence within 6 months of their initial diagnosis.[14] This results in a significant economic impact, approximately two billion dollars in the U.S. alone,[13] associated with these common and painful infections. The majority of UTIs (85−95%) are caused by members of the *Enterobacteriaceae* family; UPEC are isolated in approximately 80−85% of community-acquired UTI, and other *Enterobacteriaceae* account for 5−10% of infections.[15] Because of the increasing prevalence of recurrent infections, as well as the increasing emergence of antibiotic resistant strains,[16] including multidrug resistant UPEC such as the ESBL (extended spectrum β-lactamase) strain ST131,[17] the desire for new UTI therapeutics has escalated rapidly in recent years. The requirement for FimH to cause disease has led to its classification as a promising and validated therapeutic target[18] for UTI and, more recently, for Crohn's disease.[19] Inhibition of FimH function and activity circumvents bacterial bladder cell adhesion, invasion, and subsequent intracellular biofilm formation, making the bacteria unable to cause or propagate an existing infection.

We have previously developed[20] small molecule glycosides based on α-D-mannose (O-mannosides), such as **1** and **4** (Figure 1), as tight-binding ligands and potent antagonists of FimH both in vitro and in animal models of UTI. Although, phenyl α-D-mannosides were first reported by Firon and Sharon in the 1980s as inhibitors of yeast agglutination by mannose-specific enterobacteria,[21] the true viability of synthetic mannosides as oral therapeutics for treatment of UTI was not validated in vivo until 2010,[20a,22] where the oral activity of several biphenyl α-D-mannosides in animal models of acute and chronic UTI was demonstrated. Since then, other related mannosides have also been reported[23] and glycodendrimer[24] FimH antagonists. X-ray crystallographic data of mannosides binding to the FimH lectin domain has aided in the rational design of higher affinity ligands, with improvement gained through interactions to the "tyrosine gate" at the periphery of the deep mannose binding pocket[6c,8,20c] and to a small hydrophobic pocket[20b,23a,25] near the mannoside glycosidic bond. While O-mannosides have good efficacy in animal models of UTI, they have low bioavailability and half-life, which can possibly be attributed to the metabolic instability of the O-

glycosidic bond[20b] to either hydrolysis in the stomach or intestinal tract or, alternately, from the enzymatic action of mannosidases.

In this article, we specifically address and eliminate this potential metabolic liability of O-mannosides with new C-mannosides, which have the labile O-glycosidic bond replaced with stable carbon-based linkers to the aglycone portion of the mannoside. Herein, we report on a novel, stereoselective, synthetic route to construct this new class of biaryl, C-glycoside FimH antagonists, which encompass a unique R-hydroxy methylene bond to the aglycone. We have employed X-ray crystallography and computational docking studies of manno-sides to develop a pharmacophore model of stereospecific C-mannoside binding to FimH. Furthermore, we show that relative to O-mannosides, these new C-mannosides have greatly increased compound exposure, which we postulate to result from an increase in metabolic stability of the glycosidic bond. Exactingly, C-mannosides also have significantly improved in vitro FimH activity and in vivo efficacy in animal models of UTI.

## ■ RESULTS AND DISCUSSION

N-, S-Linked Mannosides. At the onset of this work, we synthesized two compounds, one containing a nitrogen (**2**) and the other a sulfur atom (**3**) in place of the oxygen glycosidic bond (**1**) (Figure 1). As shown in Scheme 1A, these S- and N-

## Scheme 1. Synthesis of N-, S-, and Triazole-Linked Biphenyl Mannosides[a]
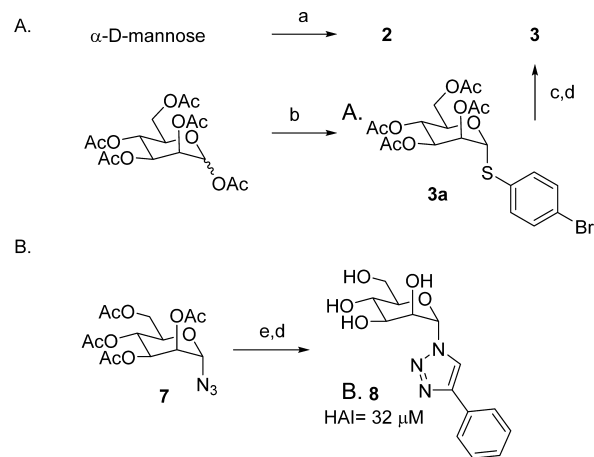
[a]Reagents and conditions: (a) methyl 4′-aminobiphenyl-3-carboxylate, EtOH, 55 °C; (b) 4-bromobenzenethiol, BF₃−OEt₂, DCM, 0 °C to rt; (c) 3-methoxycarbonylphenyl boronic acid, Pd(PPh₃)₄, Cs₂CO₃, dioxane/water (5/1), 80 °C; (d) NaOMe/MeOH, 0 °C to rt; (e) phenylacetylene, CuSO₄, Na ascorbate, EtOH/H₂O (4/1), rt.

Scheme 2. Synthesis of C-Linked Amide Mannosides[a]
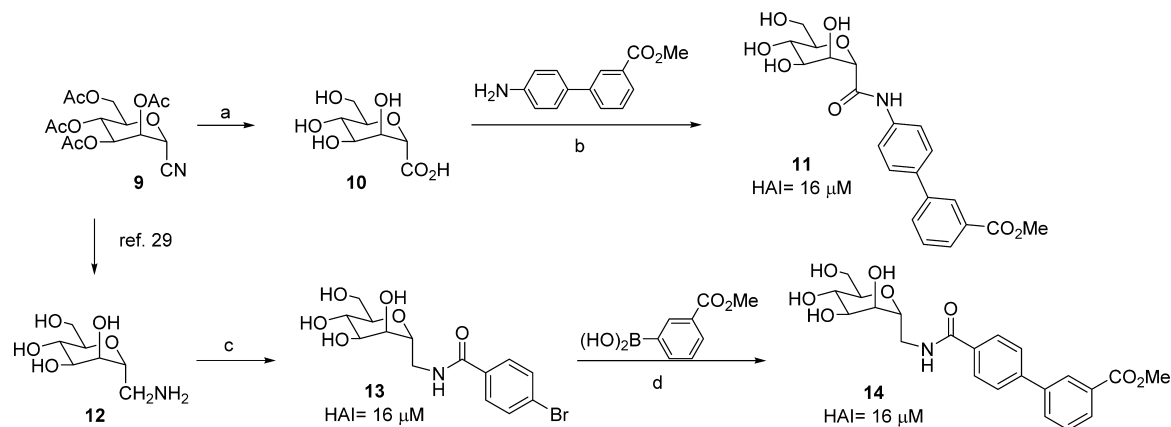
[a]Reagents and conditions: (a) 25% HCl aq, 50 °C; (b) HATU, DIPEA, 0 °C to rt, DMF; (c) 4-bromobenzoyl chloride, pyridine, rt; (d) Pd(PPh₃)₄, Cs₂CO₃, dioxane/water(5/1), 80 °C.

Scheme 3. Synthesis of C-Linked Methylene and Hydroxy-Methylene Mannosides[a]
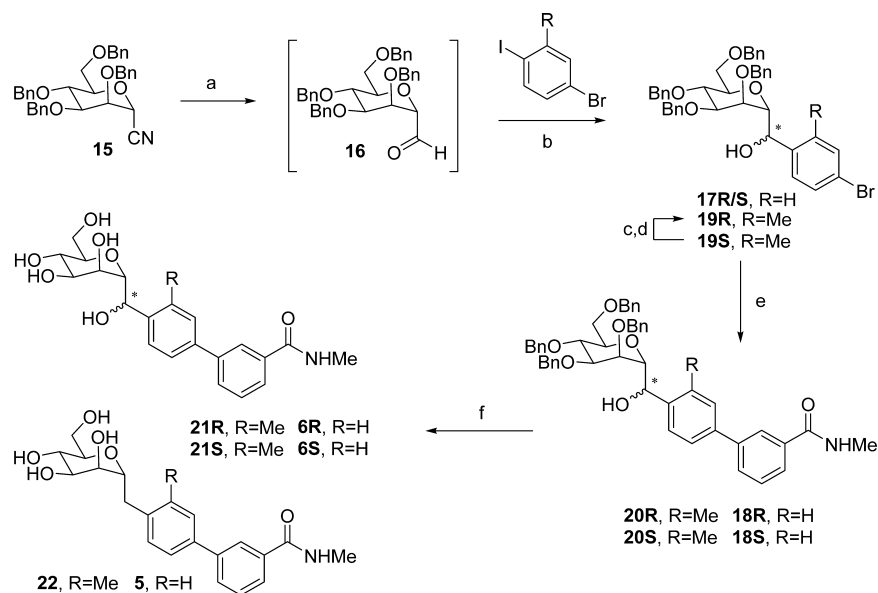
[a]Reagents and conditions: (a) DIBAL, CH₂Cl₂, −78 °C; (b) diethyl ether, −78 °C to −20 °C; (c) Dess−Martin periodinane, pyridine, CH₂Cl₂, 0 °C; (d) Li(ᵗOBu)₃AlH, THF, −40 to 0 °C; (e) 3-(N-methyaminocarbonyl)phenylboronic acid pinacol ester, Pd(PPh₃)₄, Cs₂CO₃, dioxane/water (5/1), 80 °C; (f) 10% Pd/C, H₂, MeOH, rt.

mannosides were prepared using a traditional glycosylation methodology with slight modification, first coupling α-D-mannose with methyl 4′-aminobiphenyl-3-carboxylate to give N-linked mannoside **2**, then glycosylating mannose-pentaacetate with 4-bromobenzenethiol to give **3a**, followed by a Suzuki reaction with 3-methoxycarbonylphenyl boronic acid and deprotection to give S-linked mannoside **3**. We found that both analogues had slightly lower activity (HAI = 4 μM) to that of O-mannoside **1** when tested in a hemagglutination (HA) inhibition assay using the clinical *E. coli* strain UTI89. To help guide our SAR, we also tested **2** and **3** in an isothermal shift melting point assay and found that they had equivalent binding affinity to FimH, relative to **1**. Next, we synthesized an N-linked heterocycle, triazolomannoside, via "click" chemistry methodology. Shown in Scheme 1B, the reaction of azido mannoside **7**[26] with phenylacetylene and copper sulfate, followed by sodium methoxide deacetylation, gave phenyl triazole manno-

side **8** in good yield. However, mannoside **8** lost substantial potency relative to **1**, only exhibiting an HAI of 32 μM.[27] On the other hand, it was shown by another group that **8** still retains good FimH binding affinity (IC₅₀ = 0.25 μM) as determined in a competitive binding assay.[28] Hoping to build from these initial results with N- and S-mannosides, we aimed to construct potentially more metabolically stable, carbon-based linkers, or C-mannosides.

C-Linked Amide Mannosides. Because of ease of synthesis, we first targeted a series of simple C-linked amide mannosides. Shown in Scheme 2, cyano mannoside **9**[29] was obtained by reaction of mannose pentaacetate with trimethyl-silyl cyanide and boron trifluoride diethyl etherate to give **9** as a 2:1 mixture of α and β isomers. Compound **9** was then hydrolyzed to carboxyl mannoside **10** by heating in 25% aq HCl for 2 days. 1-[Bis(dimethylamino)methylene]-1H-1,2,3-triazolo[4,5-b]pyridinium 3-oxid hexafluorophosphate (HATU)
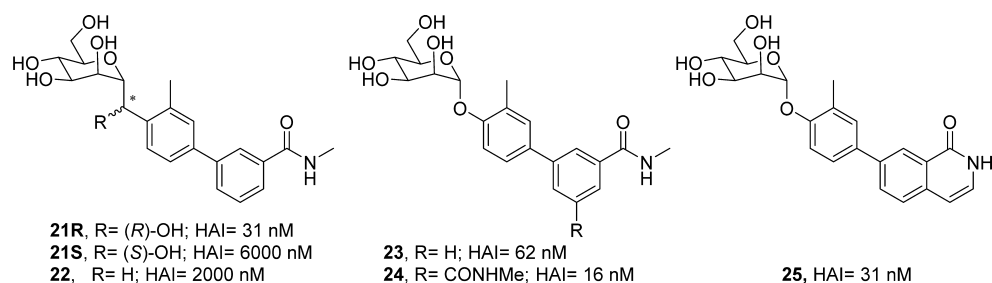
21R, R= (R)-OH; HAI= 31 nM
21S, R= (S)-OH; HAI= 6000 nM
22, R= H; HAI= 2000 nM

23, R= H; HAI= 62 nM
24, R= CONHMe; HAI= 16 nM

25, HAI= 31 nM

Figure 2. Direct comparison of the potencies of *C*-linked methylene mannosides **21R**, **21S**, and **22** to those of similar *O*-mannoside analogues **23**, **24**, and **25**.
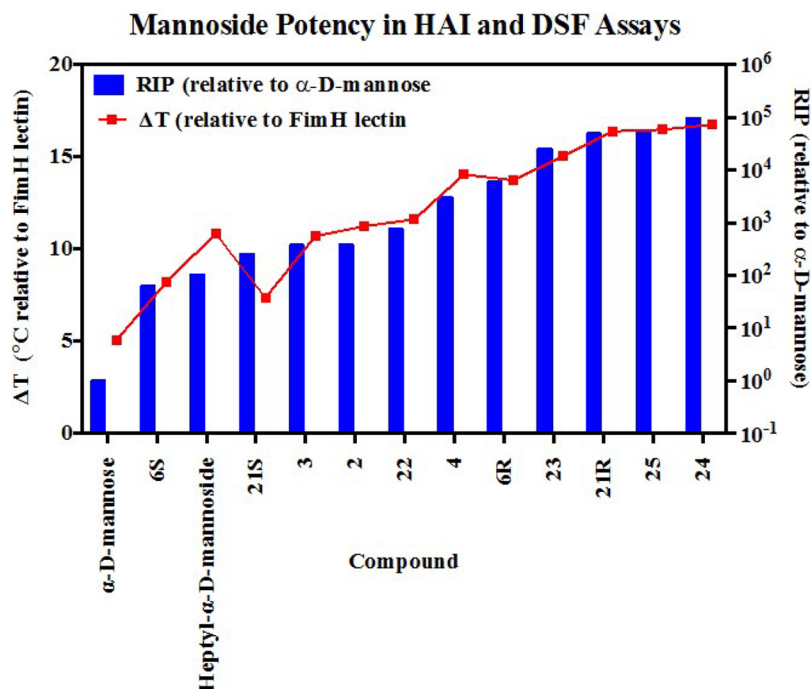

Figure 3. In vitro analysis of mannoside potency. The difference in the conformational stability of the FimH lectin domain in the presence of mannoside compared to that in the absence of mannoside, as determined by differential scanning fluorimetry, is presented on the left axis. Measurement of the melting temperature is described in the methods. The hemagglutination inhibition data is presented relative to D-mannose on the right axis and is described in the methods.

mediated coupling of **10** with methyl 4′-aminobiphenyl-3-carboxylate yielded the target *C*-linked amide mannoside **11**. In parallel, we pursued methylene spaced amides in order to investigate the effect of length and flexibility of the linker. Thus, starting from cyano mannoside **9**, we synthesized aminomethyl mannoside intermediate **12**.[30] Acylation with 4-bromo-benzoyl chloride gave amide mannoside **13**, which was coupled to methoxycarbonylphenylboronic acid via Suzuki reaction, to give methylene-spaced amide **14** as a matched pair of **1**. Testing of **11**, **13**, and **14** in the HA assay revealed that all analogues had reduced potency, relative to **1**, with HAIs of 16 μM. We rationalized that these, and the triazole linker **8**, do not allow sufficient flexibility to mimic the conformation, or key FimH binding interactions, observed for *O*-mannoside **1**. Hence, we next pursued direct methylene (CH$_2$) spaced *C*-mannosides, which provide a closer structural match to *O*-, *N*-, and *S*-mannosides **1**−**3**.

Direct Methylene *C*-Linked Mannosides. Methylene-spaced, *C*-mannoside analogues of *O*-mannoside **4** and *ortho*-methylated *O*-mannoside **23** were obtained using a newly developed, multistep synthetic procedure, starting from nitrile

15 (Scheme 3). The non-*ortho* substituted analogues were synthesized first. Bromide intermediates **17R** and **17S** were constructed in a one-pot, two-step sequence, first reducing nitrile **15** to aldehyde **16** with DIBAL, followed by the addition of an organolithium reagent (formed by lithiation of 1,4-dibromobenzene (R = H, step b). The organolithium addition yielded a mixture of alcohol isomers (**17R** and **17S**), which were separable by silica gel chromatography. Following a palladium-mediated cross-coupling of **17R** and **17S** with 3-(*N*-methylaminocarbonyl)phenyl boronate, **18R** and **18S** were obtained in good yield, respectively. Subsequent benzyl deprotection produced methylene-linked *C*-mannosides **5**, **6R** and **6S**. Following testing in the HA assay, we discovered that methylene-spaced analogue **5** (HAI = 1 μM) was equipotent to its matched pair *O*-mannoside **4** (HAI = 0.5 μM) (Figure 1). Surprisingly, we found the secondary alcohol isomers **6S** and **6R** showed differential potency, with a pronounced stereochemical preference for the *R*-hydroxyl group for FimH binding affinity. The isomer **6S** had 25-fold less potency in the HA assay (HAI = 24 μM) than **5**, whereas isomer **6R** gained 4-fold activity (HAI = 0.25 μM).

Scheme 4. Structures and Synthesis of Prodrug Analogues of *O*-Mannoside 23[a]
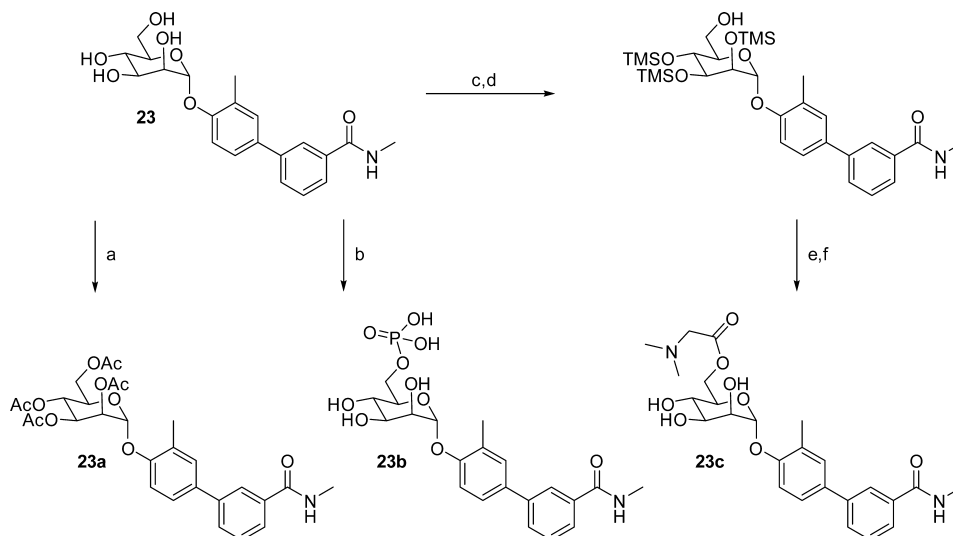
[a]Reagents and conditions: (a) Ac$_2$O, pyridine, rt; (b) POCl$_3$ trimethylphosphate, H$_2$O, 0 °C; (c) TMSCl, Et$_3$N, DMF, 0 °C; (d) AcOH, acetone/MeOH, 0 °C to rt; (e) *N,N*-dimethylglycine hydrochloride, DMAP, DIC, CH$_2$Cl$_2$/DIPEA, rt; (f) TFA, CH$_3$CN, 0 °C.

On the basis of these key results, we synthesized the *ortho*-methyl analogues **22** and **21** based on our lead *O*-glycoside **23** (Figure 2).[20a] Shown in Scheme 3, *C*-mannosides **21** and **22** were constructed in a similar fashion as for **5** and **6**, only differing in the organolithium reagent (4-bromo-2-methyl-iodobenzene [R = Me, step b]) used for the addition to aldehyde **16**. We discovered that methylene *C*-mannoside **22** (HAI = 2 μM) had a 30-fold decrease in activity relative to **23**, which is in contrast to the results obtained from **5**, which retained activity relative to its matched pair, **4**. However, we did discover the same *R*-stereospecificity of the benzylic alcohols observed with **6R** and **6S** also exists in the more potent *ortho*-methyl series, with *C*-mannoside **21R** having an HAI of 30 nM (relative to 62 nM for **23**) and S-isomer **21S** having an HAI of only 24 μM. This striking increase in the FimH activity of *R*-isomers **6R** and **21R** was attributed exclusively to a change in their relative FimH binding affinities when compared to **6S** and **4** and **21S** and **23**, respectively (Figure 3). It should be noted that although the *R* and *S* stereochemical assignment of the hydroxymethylene linker in **6** and **21** were only speculation at this time, we later confirmed the stereochemistry through small molecule X-ray crystal structure of a derivative of a key precursor, **19R** (Figure 6). From the vast potency difference seen between **21R** and **21S**, we can also presuppose that our potency-based assignments are correct for the less effective **6R** and **6S** compounds.

Stereoselective Methodology for Recycling the Undesired 19S-Isomer into the 19R-Isomer. To improve upon our yield of *R*-hydroxybenzyl *C*-mannosides, we explored alternate synthetic strategies. In this study, we sought to maximize the yield of **19R** in step d, depicted in Scheme 3, which generates a mixture of diastereomers, yielding **19R** in only 16%, and the **19S** isomer in 20%. We first investigated modified reaction conditions, including a systematic evaluation of solvents. However, these changes resulted in a lower reaction yield and also gave rise to an inseparable 4-iodo-3-methyl byproduct. Variation of other reaction parameters, such as temperature, concentration, additives, and order of addition, were also attempted, but these unproductively increased the **19S** isomer ratio. As a possible solution, we envisioned a

transformation to convert **19S** into the desired **19R** isomer. Therefore, we implemented a two-step oxidation and selective reduction protocol, allowing us to efficiently recycle the undesired **19S** isomer into **19R**. This stereoselective recycling method improved the *R:S* ratios from 1:1.2 (steps c,d) to 28:1 (steps c–f), also increasing the overall yield of **19R** from 16% to 28% (calculated from compound **15**). The oxidation of **19S** (or unresolved mixtures of **19S** and **19R**) was carried out using Dess–Martin periodinane in pyridine to give the aryl ketone intermediate **19a** (not shown) in 74%. Stereoselective reduction using the bulky lithium tri-*tert*-butoxyaluminum hydride reagent in THF gives **19R** with a respectable 17:1 (*R:S*) diastereoselectivity and an excellent yield of 84%. Upon further investigation, we elucidated that the corresponding bulky potassium tri-*sec*-butylborohydride (K-selectride), the unhindered lithium aluminum hydride (LAH), and sodium borohydride (NaBH$_4$) reagents all favored stereoselectivity for the undesired **19S** isomer. This strongly suggests that the stereoselectivity for the hydride delivery, and reduction comes from a combination of both steric and electronic interactions between the chirality of the α-D-mannoside and the chosen reducing agent. A careful review of the literature reveals that this particular use of mannose, or any other sugar, as a chiral director for the stereoselective reduction of ketones has not been reported to date and could be precedent for further investigation. We surmise that this methodology could be applied to other glycoside systems to effect a large array of diastereoselective or possibly even enantioselective ketone reductions.

Prodrugs of Mannosides. In a parallel strategy to improve the oral bioavailability and half-life (compound exposure) of *O*-mannosides, we designed and synthesized various prodrugs[31] of lead *O*-mannoside **23**. The prodrugs include tetraacetate **23a**, the 6-position phosphate **23b**, and dimethylglycine acetate **23c** (Scheme 4). Although **23a** is the precursor in the synthesis of **23**,[20b] it was synthesized by reacetylating mannoside **23**. To selectively phosphorylate the 6-position, as in prodrug **23b**, mannoside **23** was reacted with phosphoryl chloride (POCl$_3$) in water and trimethyl phosphate. Finally, prodrug **23c** was constructed via silylation of **23**, followed by selective
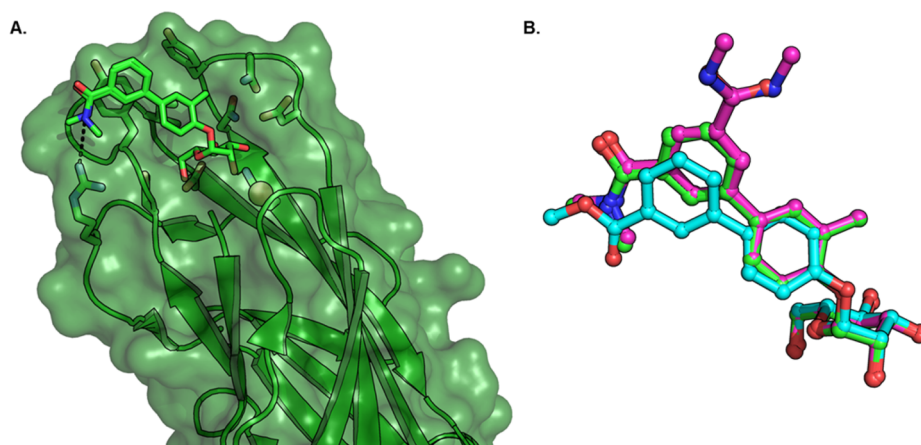
Figure 4. (A) X-ray structure of **23** bound to FimH (PDB 5F3F). Water-mediated H-bond of amide carbonyl to Y48. (B) Overlay of **23** with **24** (PDB 5F2F) and **1** (PBD 3MCY). Altered biphenyl ring conformation and amide carbonyl orientation of ortho-substituted mannosides **23** and **24** compared to **1**.
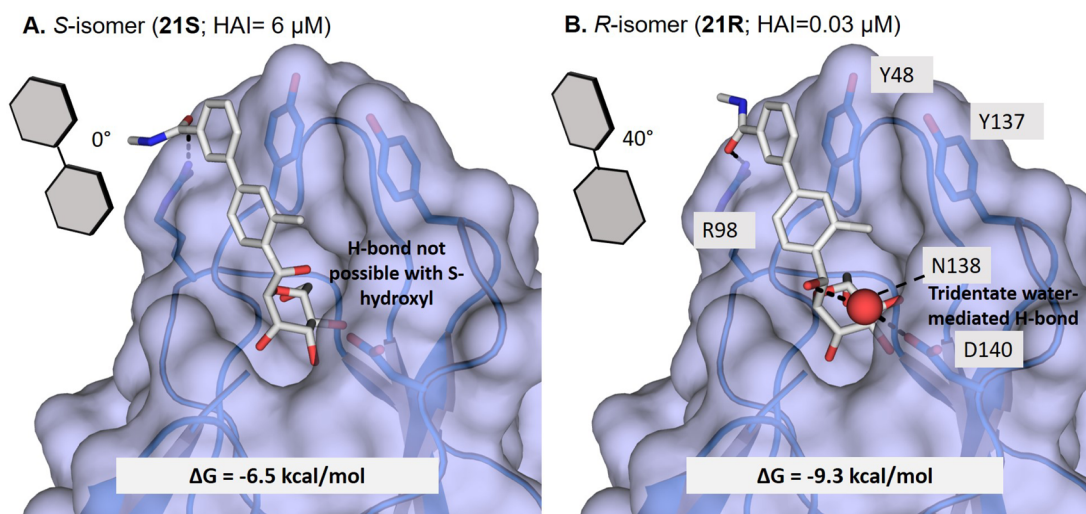

Figure 5. Computational docking models of isomeric *C*-mannosides: (A) *S*-hydroxy (**21S**) and (B) *R*-hydroxy (**21R**) bound to the FimH mannose-binding pocket. The accepted model of **21R** is bound to FimH through water-mediated H-bond to D140 and N135.

deprotection of the primary trimethylsilyl group. Next, coupling of the free 6-hydroxy group with *N,N*-dimethylaminoglycine was achieved using *N,N*-diisopropylcarbodiimide (DIC) to give prodrug **23c** upon protecting group removal with TFA.

X-ray Crystallography and Computational Modeling. To better understand the molecular interactions of *O*-mannosides **23** and its matched disubstituted analogue **24** (Figure 2)[20b] with FimH, and to help us design improved mannosides based on *C*-mannoside **21R**, we obtained co-crystal structures of **23** and **24** bound to FimH. A high-resolution 1.67 Å X-ray crystal structure of **24** (PDB 5F2F)[25] and a 1.75 Å structure of **23** (PDB 5F3F) bound to the FimH lectin domain were obtained (Figure 4A) and used to develop a pharmacophore model for mannoside FimH ligands. The *O*-linked aglycone projects toward the "lid" of the binding pocket, which engages in favorable hydrophobic and H-bonding interactions. The *ortho*-methyl substituent on the biphenyl A-ring makes hydrophobic interactions in a small pocket formed by I52, Y137, and N138. The biphenyl B-ring forms favorable π−π stacking interactions with Y48, and the *meta*-substituted amide also makes polar contacts with FimH. For example, the carbonyl of the amide forms a predicted electrostatic or H-

bonding interaction with the neighboring salt bridge, R98, and/or Y137 residues. In Figure 4B, comparison of mannosides **23** and **24** to non-*ortho*-substituted **1** (PDB 3MCY),[20c] highlights a marked difference in the biphenyl group B-ring conformation upon installation of the *ortho*-methyl group. On the basis of this new X-ray structure of **23** and previously reported structures,[23a,25,32] it is apparent that the hydrophobic contacts of the *ortho*-substituents within the small pocket, and the resultant twisted B-ring conformation, improves π−π stacking in the "tyrosine gate" with Y48 and Y137.

Computational Docking of *C*-Mannosides to FimH. Because we have not been able to obtain a co-crystal structure of *C*-mannoside **21R**, we have formulated a computational binding model, shown in Figure 5. As seen in the structure of **23** (Figure 4A), there is a crystallized water molecule between the glycoside anomeric oxygen and the D140 and N135 FimH side chains. The location of the water suggests it is involved in a H-bonding interaction between the anomeric oxygen and FimH. Our computational docking model of the diastereomers **21S** and **21R** indicates that the *R*-isomer (**21R**, Figure 5B) is favored energetically over the *S*-isomer (**21S**, Figure 5A) due to a productive water-mediated H-bond in the former. This same
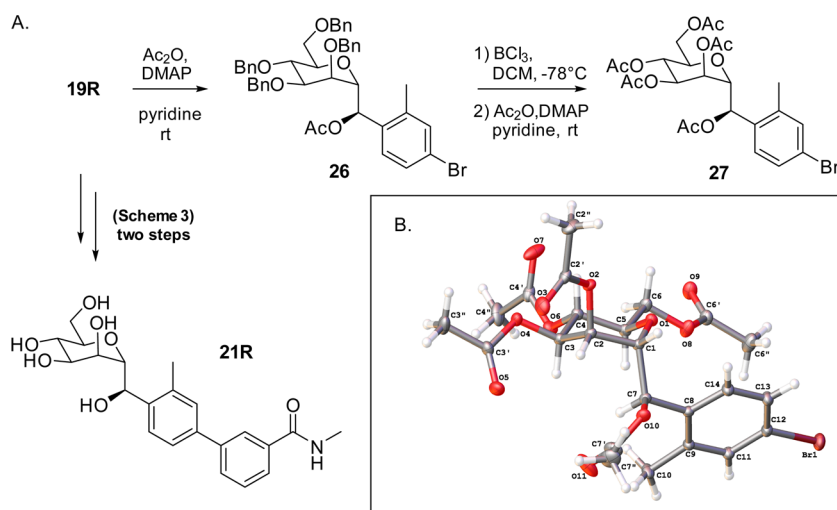
Figure 6. (A) Derivatization of key building block **19R** (precursor to **21R**). (B) Small molecule X-ray structure of acetylated intermediate **27**, confirming the *R*-stereochemistry of the **21R** benzylic hydroxyl group.
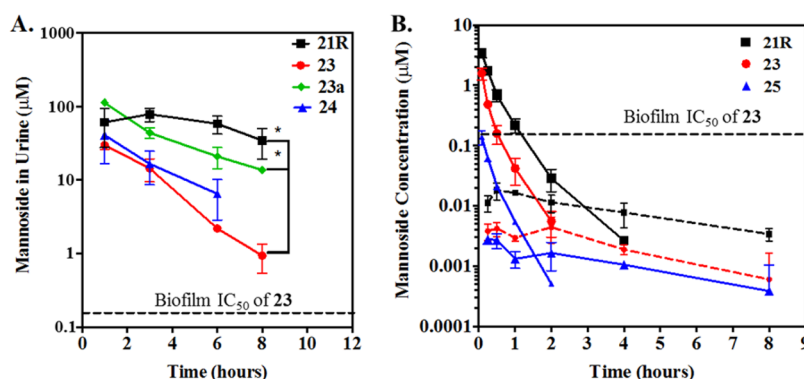

Figure 7. (A) Mannoside levels were quantified in the urines of mice over a period of 8 h following oral gavage of drug as described in the methods. Data is presented as the mean and standard deviation from at least three independent experiments. Differences in concentration at the 8 h time point were tested for significance using Mann−Whitney U test. (* *P* < 0.05). (B) Measurement of mannoside in the plasma of rats following either a 10 mg/kg oral dose (dashed lines) or a 3 mg/kg intravenous dose (solid lines). Details regarding the measurement of mannoside are described in the methods.

water molecule, positioned between the hydroxyl group of the *R*-isomer and residue(s) D140 and N135, is not accessible to the *S*-isomer. This preference is also predicted from thermodynamic calculations, as the calculated ΔG of binding for the *R*-isomer is favored by 2.8 kcal/mol over that of the *S*-isomer. These observations can explain the strong stereospecific preference for FimH binding the *R*-isomer, relative to the *S*-isomer, and why methylene spaced mannoside **22** loses activity[33] compared to *O*-mannoside **23**, as the CH_2 is not able to participate in H-bonding to this water molecule. In the absence of X-ray crystallography data of FimH binding, we determined the stereochemistry of the **21R** benzylic hydroxyl by obtaining a small molecule X-ray crystal structure of crystalline *C*-mannoside aryl bromide intermediate, **27** (Figure 6). The high resolution X-ray of **27** unequivocally confirms that the benzylic hydroxyl group of intermediate **19R**. By logical deduction, **19R** and its final product **21R**, both have the *R*-stereochemistry, reinforcing our computational docking model invoking a stereospecific water-mediated H-bond to FimH.

Pharmacokinetics (PK) of Mannosides. To further examine the therapeutic potential of the new *C*-mannosides and *O*-mannoside prodrugs, we evaluated their pharmacokinetic (PK) behavior in vivo. Mannosides were delivered orally

in a suspension of 10% cyclodextrin. Previous administration utilized DMSO as a vehicle. Our decision to administer in cyclodextrin was 2-fold: (1) cyclodextrin is commonly used for increasing the aqueous solubility and bioavailability of drugs[34] and (2) DMSO has been demonstrated to modulate the host immune response, obfuscating any observed results.[35] The concentration of mannoside detected in the urine of mice was monitored at multiple time points following oral delivery over a period of 8 h and quantitatively measured by HPLC and mass spectrometry. As previously published, *O*-linked mannosides, including both **23** and **24**, were found to accumulate at high concentrations in the urine as early as 1 h post dosing,[20b] followed by a steady almost linear decrease throughout the collection time frame (Figure 7A). Despite this continual decrease in concentration, the relative concentration of each mannoside remained well above the HAI EC_{90} (0.062 μM) and biofilm IC_{50} (0.15 μM) of **23** throughout this period. In contrast to **23** and **24**, the concentrations of **21R** and **23a** (the acetate prodrug of **23**) remained substantially higher throughout the period measured, resulting in a significantly increased AUC. Shown in Figure 7A, the concentration of both **21R** and **23a** in the urine 8 h following oral delivery was significantly higher than **23**. Compound levels of **21R** reached

Table 1. Compound Structures and Comparison of Biological Activity and Physical Properties Between *O*- and *C*-Mannoside Matched Pairs (ND = not determined)

Compound Name	Structure	Molecular Weight (g/mol)	cLogP	HAI EC$_{90}$ (µM)	DSF Melting Temp (°C)	Biofilm Prevention IC$_{50}$ (µM)
4		389.4	0.28	0.500	73.2	1.35
6R		403.4	-0.48	0.250	72.8	0.90
6S		403.4	-0.48	24.000	67.2	38.0
23		403.4	0.93	0.062	74.5	0.15
21R		417.4	-0.15	0.031	75.4	0.08
21S		417.4	-0.15	6.000	66.4	11.0
30		415.4	1.04	0.032	75	0.25
29R		429.5	-0.03	0.008	76.5	0.04
25		413.4	1.4	0.031	75.4	0.13
28R		427.4	0.32	0.006	77.5	0.03
33		412.4	2.28	0.020	75.1	0.34
31R		426.5	1.2	0.006	77.7	0.04
34		397.4	1.2	0.062	75.0	0.14
32R		411.4	0.14	0.125	74.6	0.60

50 µM at 8 h, which is *1600 times higher than its HAI potency*. Acetate prodrug **23a** also showed enhanced concentration, presumably from higher gut permeability, resulting in a 20-fold higher concentration (20 µM) of **23** relative to direct oral dosing of **23** (1 µM) at 8 h.

To further expand on this result, we conducted a more thorough examination of the PK properties of **23** and **21R** as well as the analogous ring-constrained isoquinolone *O*-mannoside **25**[25] (Figure 2) in rats (Figure 7B). Recent examination of the PK behavior and efficacy of **25** in mice identified it as a leading therapeutic candidate in the *O*-mannosides series.[25] In contrast to the previous study (Figure 7A), here we monitored the concentration of mannoside in the plasma of rats following either a 10 mg/kg oral dose (dashed lines) or a 3 mg/kg intravenous dose (solid lines) (Figure 7B). Analysis of the rat PK data revealed that, while *C*-mannoside **21R** encompassed the highest level of compound exposure (as assessed by C_{max} and AUC_{all}) and the lowest clearance rate, at 34.9 mL/min/kg (**23** clearance rate = 98.4 mL/min/kg) *O*-mannoside **25** shows the highest clearance rate (408 mL/min/kg) and volume of distribution (V_{dss} = 6.7 L) but the highest bioavailability (7%) of all compounds tested. This suggests that

the biaryl B-ring isoquinolone aglycone of **25** significantly enhances permeability in the gut, while on the other hand, *C*-mannoside **21R** and the *O*-mannoside prodrug **23a** have a longer half-life and extended compound exposure, presumably from a combination of increased bioavailability from the prodrugs and metabolic stability of the *C*-mannoside. Because *O*-mannosides **24** and **25** were stable ($t_{1/2}$ > 2h) in plasma, simulated gut fluid (pH 1.2), simulated intestinal fluid (pH 6.8), and liver microsomes, we hypothesize that the increased exposure of *C*-mannoside **21R** is likely due to evading the enzymatic action of mannosidases. This combined data constitutes key structure−property relationships (SPR) and was useful for guiding further optimization of the *C*-mannosides described below.

Synthesis of Optimized *C*-Linked Isoquinolone Mannosides. Inspired by the enhanced potency and increased compound exposure of *C*-mannoside **21R**, coupled with the improved oral bioavailability of **25**, we synthesized its *C*-mannoside matched pair analogue, **28R**. Suzuki cross-coupling between **27** and 1-hydroxyisoquinoline-7-boronate ester, followed by acetyl deprotection, generated biaryl isoquinolone *C*-mannoside **28R** (Table 1). In an alternate synthesis, **19R** was
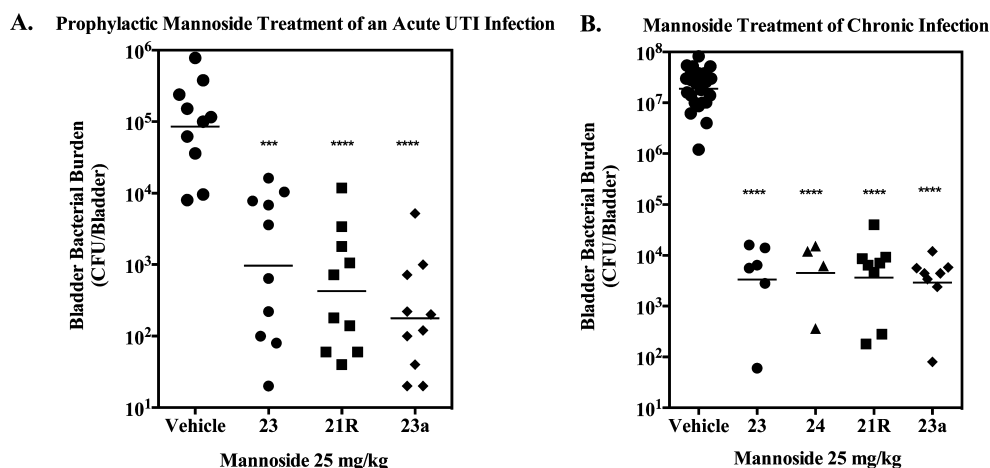
Figure 8. (A) Prophylactic treatment of an acute UTI. Mannoside was dosed orally at 25 mg/kg in 10% cyclodextrin, 30 min prior to infection with 10^7 CFUs UPEC. Bladders were harvested 6 h postinfection and bacterial burdens enumerated. (B) Mannoside treatment of chronic UTI. Mice were treated orally with 50 mg/kg of mannoside in 10% cyclodextrin, after 14 days of chronic UPEC infection. Bladders were harvested 6 h following oral dosing and bacterial burdens enumerated. Data from at least two independent experiments are presented in each panel; bars indicate geometric means. Differences between treated groups and vehicle were tested for significance using Mann−Whitney U test (*** $P = 0.0001$, **** $P < 0.0001$).

used in place of **27** in the Suzuki reaction, but attempts to remove the benzyl protecting groups via hydrogenation resulted in formation of the saturated dihydroisoquinolone analogue **29R**. For direct comparison, we repeated this hydrogenation on *O*-glycoside **25** to give corresponding analogue **30**. We found that both isoquinolone **28R** and dihydroisoquinolone **29R** have excellent potency, with HAI titers of 8 and 6 nM, respectively. This equates to a ~4.5-fold increase in potency over the *O*-mannoside matched pairs, **25** and **30** (HAI = 31 and 32 nM, respectively). Following these exciting results, we evaluated fused ring systems like **25** that would still retain their H-bonding and FimH binding attributes. Using similar procedures as described above, we synthesized aminoisoquinoline **31R** and isoquinoline **32R**, both possessing a nitrogen atom that occupies a position equivalent to the carbonyl oxygen on the isoquinolone ring of **25**. Isoquinoline **32R** has a different ring fusion, being attached to the aglycone A-ring at the 5-position (versus the 7-position in **31R**, **28R**, and **29R**). As expected, the *C*-mannoside **31R** was 3-fold more potent than its matched *O*-mannoside pair **33**, with an HAI of 6 nM. However, the 5-position isoquinoline *C*-mannoside **32R** had lower potency relative to its *O*-mannoside pair **34**[24] (HAI = 62 nM), with an HAI of 125 nM (Table 1). This unexpected result can be rationalized from docking studies (not shown), wherein we found that due to a dramatic shift in ring conformation of the *C*-mannosides relative to the *O*-mannosides (Figure 5), a steric clash exists between FimH and this 5-position ring substitution of **32R** in the *C*-mannoside series, which does not exist in **34** of the *O*-mannoside series. When comparing the matched pair *C*- and *O*-mannosides shown in Table 1, it is apparent that the cLogP values are approximately 1 Log unit lower in the *C*-mannoside series. For example, comparing **33** to **31R**, we see a drop in cLogP from 2.28 to 1.2, respectively, suggesting that **31R** has respectable oral drug-like physical properties like **25** (cLogP 1.4) but with enhanced glycosidic bond stability.

In Vivo Efficacy of Mannosides in Acute and Chronic Cystitis. Given the improved in vivo PK behavior of both the *C*-mannoside **21R** and the prodrug **23a**, we next investigated whether these enhancements improved their potency in animal models of UTI.[20a,36] The distinct pathophysiology of UTI that

has been identified in these murine models has also been observed in humans, demonstrating their relevance.[37] To measure efficacy in these models, we examined the ability of mannosides to *prevent* the initial pathogenic steps of UPEC infection in our prophylactic model of acute UTI as well as their ability to *treat* an established infection in our model of chronic UTI. Despite the disparity in potency and PK behavior, the efficacy of all the compounds, in either model, were nearly identical (Figure 8). When tested as a prophylaxis therapy (Figure 8A), where the mannoside is dosed 30 min prior to UPEC infection and bacterial titers enumerated 6 h post-infection, tetraacetate prodrug **23a** and phosphate prodrug **23b** (see Supporting Information data) each showed improved efficacy compared to **23**. In contrast, the glycine acetate prodrug **23c** (see Supporting Information data) did not show enhanced efficacy, perhaps due to its increased stability in conversion to drug or decreased oral absorption in the gut relative to **23a** and **23b**.

Both the *O*-linked and *C*-linked mannosides accumulated in the urine at concentrations over 10-fold higher than their HAI EC_{90} and biofilm IC_{50} (Figure 7) up to 8 h following oral dosing. Thus, we hypothesized that 6 h post-treatment was too early to discriminate relative mannoside potency in the chronic UTI model (Figure 8B). To investigate this possibility, we first monitored the pharmacodynamics (PD) of *O*-linked manno-side **24** in our treatment model of chronic UTI to evaluate its therapeutic window. Diamide mannoside **24** has similar PK to monoamide mannoside **23** but was found to be 4-fold more potent in our HA assay (HAI = 16 nM), identifying it as one of our most effective *O*-linked mannosides in vitro. Following oral delivery of **24** in the chronic UTI model, we found a significant decrease in bladder burden from 10^7 CFUs to approximately 10^5 CFUs 2 h postdosing (Figure 9). Bladder burdens continued to decrease to 10^4 CFUs at 6 h but leveled off at 12 hours, when the geometric mean of the bacterial burden increased to 10^5. Interestingly, the 12-hour time point appears to be comprised of a bimodal distribution, consisting of mice that have either high or low bacterial burdens in the bladder (Figure 9). Taken together, this data demonstrates a rapid reduction of bladder burdens following oral delivery of *O*-linked mannoside **24** and an increase of burdens in a
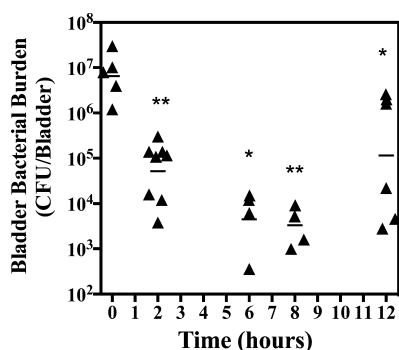
9398

Figure 9. Pharmacodynamics of *O*-linked mannoside. Chronically infected mice were treated orally with 50 mg/kg of mannoside **24**. Bladders were harvested at the designated time points following oral dosing and bacterial burden enumerated. Bars indicate geometric means. Differences between the designated time point and the 0 h time point were tested for significance using Mann−Whitney U test (* $P < 0.05$, ** $P < 0.001$).

subpopulation of mice 12 hours after treatment that may represent bladder repopulation once mannoside levels fall below the HAI.

C-Mannosides Displays Significantly Improved and Prolonged Efficacy in Vivo. Given the observed bimodal distribution of bladder burdens 12 hours after treatment with mannoside **24**, we next decided to investigate the influence of the improved pharmacokinetic behavior of *C*-mannoside **21R** on its ability to treat chronic cystitis at this time point following oral delivery of the mannoside (Figure 10A). Additionally, to accentuate any differences in efficacy at this time point, we reduced the mannoside dosages by half, treating only with a 25 mg/kg dose. At 12 h post treatment, the *O*-linked mannoside **24** resulted in a noticeable, but not significant, decrease in bladder burdens compared to vehicle. Treatment with prodrug **23a** resulted in a similar, but statistically significant, decrease in bladder burdens. In contrast, it was found that treatment with *C*-mannoside **21R** at 25 mg/kg resulted in a dramatic and significant decrease in CFUs as compared to both vehicle and *O*-linked mannosides **24** and **23a**. Indeed, bladder burdens of mice treated with **21R** were uniformly three logs lower than untreated mice, clearly demonstrating the improved efficacy of the *C*-linked mannoside.

Furthermore, using the newly optimized heterocyclic *C*-mannosides, **28R**, **29R** and **31R**, we found significantly augmented activity relative to *O*-mannoside **25** when tested

in the prophylactic model of UTI (Figure 10B), described above, where compound was dosed orally (25 mg/kg) 30 min before infection. The in vivo activity seen with **28R**, **29R**, and **31R** is similar to **21R**, but it can be argued that **29R** and **31R** perform slightly better in preventing an infection in this model of acute UTI. However, there is a clear difference in efficacy displayed between the *C*-mannosides and *O*-mannoside **25**. This is nicely illustrated by direct comparison of *O*-mannoside **25** and its matched *C*-mannoside **28R**, which decreases bacterial titers 2 Logs lower (100-fold). Taken together with the fact that *O*-mannoside **25** and *C*-mannoside **21R** are equivalent in both FimH binding (DSF = 75.4 °C) and target inhibition (HAI = 31 nM), this result suggests that the *C*-mannosides have superior metabolic stability.

CONCLUSION

Carbohydrates, and in particular small glycosides, are typically unstable in vivo due to their inherent susceptibility to hydrolysis in the stomach or intestine and to enzymatic hydrolysis by various glycosidases present in the gut, plasma, and some tissues. This instability can critically limit the oral bioavailability, half-life. and overall therapeutic potential of glycoside-based drugs[38] like FimH mannoside antagonists. The replacement of *O*-glycosidic bonds with sulfur, carbon, or nitrogen-based linkers is one strategy that can be utilized to increase the metabolic stability of glycosides while also theoretically helping to increase their bioavailability. However, the synthesis of unnatural glycoside linkers is challenging and the influence of these changes on activity are not always predictable or straightforward. In the current manuscript, we implemented a rational strategy to improve mannoside PK and efficacy by replacing the glycosidic bond of the *O*-mannosides with a number of unique carbon-based linkers that are likely stable to metabolism. To access these novel *C*-mannosides, we have designed a new stereoselective synthetic route for the assembly of hydroxymethyl *C*-mannosides. While increased stability to mannosidases is the most reasonable explanation for the improved efficacy in vivo, other properties may be contributing to this behavior. Current investigations are confirming this hypothesis through both in vitro and in vivo studies which are beyond the scope of this initial communication.

In summary, mannoside FimH antagonists represent a first-in-class antivirulence drug in the treatment of chronic UTI and the prevention of recurrent cystitis. Herein, we have rationally
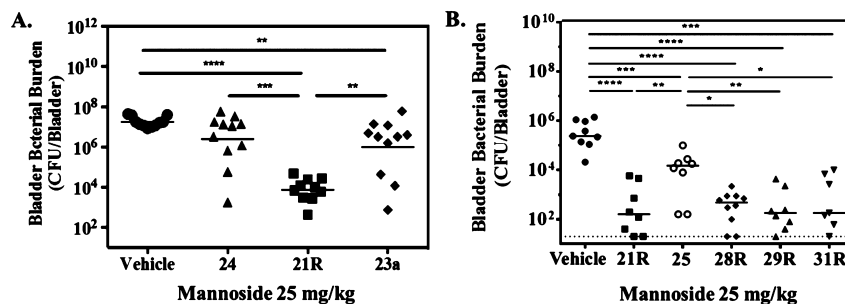
Figure 10. Improved efficacy of *C*-linked mannosides. (A) Chronically infected mice were treated orally with 25 mg/kg of mannoside. Bladders were harvested 12 hours following oral dosing and bacterial burdens enumerated. (B) Mice were treated orally with 25 mg/kg of mannoside 30 min prior to infection. Bladders were harvested 6 h following infection and bacterial burdens enumerated. Data from at least two independent experiments are presented; bars indicate geometric means. Differences between treated groups and vehicle were tested for significance using Mann−Whitney U test (**$P < 0.01$, *** $P = 0.0001$, **** $P < 0.0001$).

designed a novel *C*-mannoside FimH antagonist **21R**, which we subsequently modified, based on *O*-mannoside SAR and isoquinolone derivative **25**,[25] to generate several optimized analogues, **28R**, **29R**, and **31R**. These *C*-mannosides have become preclinical candidates for use as novel antivirulence drugs in UTI therapy.[18] Along with other lead compounds, they are currently being profiled in advanced in vivo PK, efficacy, and toxicologuey studies in preparation for selecting a lead candidate drug for clinical trials. Upon successful clinical development, a mannoside would not only represent the first small molecule FimH antagonist drug for UTI but also the first antibiotic-sparing therapeutic for the treatment of Gram-negative infections. This could also pave the way for the new development of other antibiotic-sparing drugs targeting other lectins or virulence factors, which are desperately needed for other infectious diseases.

■ EXPERIMENTAL SECTION

General Synthesis, Purification, and Chemistry Procedures. Starting materials, reagents, and solvents were purchased from commercial vendors unless otherwise noted. In general, anhydrous solvents are used for carrying out all reactions. ^{1}H NMR spectra were measured on a Varian 300 MHz NMR instrument or Varian 400 MHz NMR instrument equipped with an auto sampler. The chemical shifts were reported as δ ppm relative to TMS using residual solvent peak as the reference unless otherwise noted. The following abbreviations were used to express the peak multiplicities: s = singlet; d = doublet; t = triplet; q = quartet; m = multiplet; br = broad. Melting points were determined on a Kofler micro hot stage and were uncorrected. High-performance liquid chromatography (HPLC) was carried out on GILSON GX-281 using Waters C18 5 μM 4.6 mm × 50 mm and Waters Prep C18 5 μM 19 mm × 150 mm reverse phase columns, eluted with a gradient system of 5:95 to 95:5 acetonitrile:water with a buffer consisting of 0.05−0.1% TFA. Mass spectroscopy (MS) was performed on HPLC/MSD using a gradient system of 5:95 to 95:5 acetonitrile:water with a buffer consisting of 0.05−0.1% TFA on a C18 or C8 reversed phased column and electrospray ionization (ESI) for detection. All reactions were monitored by thin layer chromatography (TLC) carried out on either Merck silica gel plates (0.25 mm thick, 60F254) or Millipore Silica gel aluminum sheets (60F254) and visualized by using UV (254 nm) or dyes such as KMnO$_4$, *p*-anisaldehyde, and CAM (Hannesian's Stain). Silica gel chromatography was carried out on a Teledyne ISCO CombiFlash purification system using prepacked silica gel columns (12−330 g sizes). All compounds used for biological assays are greater than 95% purity based on NMR and HPLC by absorbance at 220 and 254 nm wavelengths.

General Procedure for the Suzuki Coupling Reactions (Amounts and Volumes Are Specified within Individual Procedures). Cesium carbonate (Cs$_2$CO$_3$) was activated by adding it to a round-bottom flask, which was then heated to 250 °C under vacuum for 2 min and then allowed to cool to rt under vacuum for an additional 10 min, after which time a nitrogen atmosphere was continuously maintained. Next, the desired mannosyl bromide (or mannosyl boronate ester) derivative was dissolved into dioxane and the solution was added dropwise, followed by the addition of the desired boronate-aglycone (or bromide-aglycon if mannosyl boronate was used) and, finally a small amount of water. After allowing the reaction contents to stir for 5 min at rt, a catalytic amount of tetrakis(triphenylphosphine)palladium(0) [Pd(Ph$_3$)$_4$] was added and the reaction flask was evacuated under high vacuum and backfilled with N$_2$ three times and then placed in an oil bath preheated to 80 °C and allowed to stir for the time specified (typically 1.5 h). Upon completion, the reaction was cooled to rt and solvents were evaporated under reduced pressure. The crude reaction residue was then purified and deprotected as specified.

Detailed Procedures for the Synthesis of Final Mannosides and Intermediates. *4′-(α-D-Mannopyranosylamino)-[1,1′biphen-*

yl]-3-carboxylic Acid Methyl Ester (2). α-D-Mannose (0.360 g, 2 mmol) and methyl 4′-aminobiphenyl-3-carboxylate (0.454 g, 2 mmol) were dissolved into ethanol (5 mL), and the reaction was heated to 55 °C for 17 h. After cooling down to rt, the white precipitate that formed was collected by filtration. The precipitate was washed with ethanol (2 × 3 mL) and then dried in vacuo to afford pure **2** in 77% yield. Analytical data for **2**: ^{1}H NMR (300 MHz, acetonitrile-*d*$_3$ and D$_2$O) δ ppm 3.28−3.38 (m, 1H), 3.54−3.59 (m, 2H), 3.64−3.71 (m, 2H), 3.86 (s, 3H), 3.88−3.92 (m, 1H), 4.89 (d, J = 1.1 Hz, 1H), 6.80−6.91 (m, 2H), 7.44−7.58 (m, 3H), 7.75−7.90 (m, 2H), 8.11−8.20 (m, 1H). ^{13}C NMR (100 MHz, methanol-*d*$_4$/dimethyl sulfoxide-*d*$_6$; 10/1) δ ppm 52.8, 62.8, 68.6, 72.9, 76.2, 78.9, 83.3, 115.6 (×2), 127.8, 128.1, 128.7 (×2), 130.2, 130.8, 131.7, 131.9, 142.8, 147.5, 168.4. ESI-MS found: [M + H]$^+$, 390.1.

4′-(α-D-Mannopyranosylthio)-[1,1′-biphenyl]-3-carboxylic Acid Methyl Ester (3). Step 1: Under nitrogen atmosphere at 0 °C, boron trifluoride diethyl etherate (0.427 g, 3.0 mmol) was added dropwise into a solution of α-D-mannose pentaacetate (0.390 g, 1.0 mmol) and 4-bromobenzenethiol (0.378 g, 2.0 mmol) in 6 mL of CH$_2$Cl$_2$. After 5 min, the mixture was warmed to rt and allowed to stir for 48 h. The reaction was then quenched with water and extracted with CH$_2$Cl$_2$. The CH$_2$Cl$_2$ layer was collected, dried over Na$_2$SO$_4$, and concentrated in vacuo. The resulting residue was purified by silica gel chromatography (ethyl acetate−hexanes gradient elution), giving rise to the intermediate 4-bromophenyl 2,3,4,6-tetra-*O*-acetyl-1-thio-α-D-mannopyranoside (**3a**) (0.40 g) in 77% yield. Analytical data for **3a**: ^{1}H NMR (300 MHz, chloroform-*d*) δ ppm 2.01−2.10 (m, 9H), 2.16 (s, 3H), 4.10 (dd, J = 12.1, 2.5 Hz, 1H), 4.30 (dd, J = 12.1, 6.0 Hz, 1H), 4.43−4.61 (m, 1H), 5.24−5.40 (m, 2H), 5.43−5.52 (m, 2H), 7.32−7.39 (m, 2H), 7.42−7.49 (m, 2H). ESI-MS found: [2 M + H$^+$] 1039.1.

Step 2: Following the general Suzuki-coupling procedure, mannosyl bromide **3a** (0.20 g, 0.39 mmol) from step 1, commercially available 3-methoxycarbonylphenylboronic acid (0.106 g, 0.59 mmol), cesium carbonate (0.381 g, 1.17 mmol), and tetrakis(triphenylphosphine) palladium (0.045 g, 0.04 mmol) in dioxane/water (5 mL/1 mL) were reacted under N$_2$ at 80 °C for 1 h. Upon completion, the reaction was cooled to rt, and the mixture was filtered through a silica gel column (ethyl acetate−hexanes, 2/1 isocratic elution) to remove the metal catalyst and salts. The filtrate was concentrated then dried in vacuo. To the crude residue was added MeOH (6 mL) and a catalytic amount of sodium methoxide (0.02 M), and the mixture was stirred at rt overnight. H$^+$ exchange resin (DOWEX 50WX4-100) was added to neutralize the mixture, the resin was filtered off, and the filtrate concentrated. The resulting residue was purified by HPLC [C18, 15 mm × 150 mm column; eluent, acetonitrile/water (0.1% TFA)] to give **3** (0.095 g) in 63% yield. Analytical data for **3**: ^{1}H NMR (300 MHz, methanol-*d*$_4$) δ ppm 3.66−3.91 (m, 4H), 3.94 (s, 3H), 4.01−4.16 (m, 2H), 5.51 (d, J = 1.4 Hz, 1H), 7.51−7.69 (m, 5H), 7.81−7.93 (m, 1H), 8.00 (dt, J = 7.8, 1.4 Hz, 1H), 8.24 (t, J = 1.7 Hz, 1H). ^{13}C NMR (100 MHz, methanol-*d*$_4$ /dimethyl sulfoxide-*d*$_6$; 20/1) δ ppm 52.8, 62.6, 68.7, 73.2, 73.6, 76.0, 90.2, 128.6 (×2), 128.6, 129.5, 130.4, 132.0, 132.5, 133.2 (×2), 135.9, 140.0, 141.8, 168.1. ESI-MS found: [M + H]$^+$ 407.1.

4′-[(α-D-Mannopyranosyl)methyl]-N-methyl-[1,1′biphenyl]-3-carboxamide (5). The title compound was obtained from the preparation of **6S** as a side product in 35% yield (0.005 g, 0.013 mmol). Analytical data for **5**: ^{1}H NMR (400 MHz, methanol-*d*$_4$) δ ppm 2.93−3.00 (m, 4H), 3.04−3.13 (m, 1H), 3.62−3.88 (m, 6H), 4.09−4.17 (m, 1H), 7.39 (d, J = 8.2 Hz, 2H), 7.48−7.57 (m, 1H), 7.62 (d, J = 7.8 Hz, 2H), 7.74−7.79 (m, 2H), 8.06 (br s, 1H). ^{13}C NMR (100 MHz, methanol-*d*$_4$) δ ppm 26.9, 36.1, 63.1, 69.4, 72.0, 72.7, 76.4, 80.4, 126.6, 126.9, 128.1 (×2), 130.1, 130.9 (×2), 131.0, 136.2, 139.6, 139.7, 142.6, 170.7. ESI-MS found: [M + H]$^+$ 388.2.

4′-[(α-D-Mannopyranosyl)-(R)-hydroxymethyl]-N-methyl-[1,1′biphenyl]-3-carboxamide (6R). A mixture of **18R** (0.039 g, 0.051 mmol) and 10% wt Pd/C (0.044 g, 0.02 mmol) in MeOH (10 mL) was stirred under 1 atm of H$_2$ for 16 h. The Pd/C was filtered off, and the filtrate was concentrated and dried in vacuo to give title compound **6R** (0.020 g, 0.050 mmol) in 99% yield. Analytical data for **6R**: [1]H

NMR (300 MHz, methanol-d_4) δ ppm 2.95 (s, 3H), 3.54−3.81 (m, 4H), 3.86−4.05 (m, 2H), 4.25 (t, J = 3.0 Hz, 1H), 5.01 (d, J = 8.0 Hz, 1H), 7.46−7.61 (m, 3H), 7.67 (d, J = 8.2 Hz, 2H), 7.74−7.88 (m, 2H), 8.08 (t, J = 1.7 Hz, 1H). ^{13}C NMR (100 MHz, methanol-d_4) δ ppm 27.0, 62.8, 69.0, 69.9, 72.6, 72.9, 77.8, 82.4, 126.7, 127.0, 127.8 (×2), 128.7 (×2), 130.1, 131.0, 136.2, 140.8, 142.6, 143.5, 170.7. ESI-MS found: [M + Na$^+$] 426.2.

4′-[(α-D-Mannopyranosyl)-(S)-hydroxymethyl]-N-methyl-[1,1′bi-phenyl]-3-carboxamide (6S). A mixture of **18S** (0.028 g, 0.037 mmol) and 10% wt Pd/C (0.032 g, 0.015 mmol) in MeOH (10 mL) was stirred under 1 atm of H$_2$ for 16 h. The Pd/C was filtered off, and the filtrate was concentrated and dried in vacuo. The resulting residue was purified by HPLC [C18, 15 mm × 150 mm column; eluent, acetonitrile/water (0.05% TFA)], to give **6S** (0.010 g, 0.025 mmol) in 67% yield [compound **5** was also isolated as a product in 35% yield (0.005 g, 0.013 mmol)]. Analytical data for **6S**: ^{1}H NMR (300 MHz, methanol-d_4) δ ppm 2.95 (s, 3H), 3.49−3.58 (m, 1H), 3.59−3.84 (m, 4H), 3.86−4.02 (m, 2H), 5.04 (d, J = 9.0 Hz, 1H), 7.48−7.60 (m, 3H), 7.71 (d, J = 8.2 Hz, 2H), 7.76−7.84 (m, 2H), 8.08 (s, 1H). ^{13}C NMR (100 MHz, methanol-d_4) δ ppm 27.0, 63.4, 69.1, 69.9, 71.2, 72.9, 77.1, 84.0, 126.8, 127.1, 128.3 (×2), 128.7 (×2), 130.2, 131.0, 136.2, 141.4, 142.3, 142.3, 170.6. ESI-MS found: [M + Na$^+$] 426.2.

1-α-D-Mannopyranosyl-4-phenyl-1H-1,2,3-triazole (8).[27,28] Step 1: Under a nitrogen atmosphere, ethanol/water (4 mL/1 mL) was added into the RB flask containing 2,3,4,6-tetra-O-acetyl-α-D-mannopyranosyl azide (**7**) (0.075 g, 0.20 mmol) (obtained from D-mannose pentaacetate[27]), phenyl acetylene (0.026 g, 0.24 mmol), copper(II) sulfate pentahydrate (0.01 g, 0.04 mmol), and sodium ascorbate (0.016 g, 0.08 mmol). The mixture was stirred at room temperature overnight. The solvent was removed and the residue was purified by silica gel chromatography (ethyl acetate−hexanes gradient elution), giving rise to the tetraacetate protected intermediate 1-(2,3,4,6-tetra-O-acetyl-α-D-mannopyranosyl)-4-phenyl-1H-1,2,3-tria-zole (**8a**) (0.030 g, 0.062 mmol) in 31% yield. Analytical data for **8a**: ^{1}H NMR (300 MHz, chloroform-d) δ ppm 2.05−2.12 (m, 9H), 2.20 (s, 3H), 3.89−3.99 (m, 1H), 4.08 (dd, J = 12.50, 2.61 Hz, 1H), 4.40 (dd, J = 12.50, 5.36 Hz, 1H), 5.40 (t, J = 8.79 Hz, 1H), 5.95−6.04 (m, 2H), 6.07 (d, J = 2.75 Hz, 1H), 7.34−7.53 (m, 3H), 7.79−7.92 (m, 2H), 7.96 (s, 1H). ESI-MS found: [M + Na$^+$] 498.1.

Step 2: Tetraacetate **8a** (0.028 g, 0.059 mmol) from step 1 was stirred in 6 mL of MeOH with a catalytic amount of sodium methoxide (0.02 M) at room temperature overnight. H$^+$ exchange resin (DOWEX 50WX4-100) was added to neutralize the mixture pH. The resin was filtered off, and the filtrate was concentrated and then dried in vacuo, giving rise to the title compound (0.015 g, 0.049 mmol) in 83% yield. Analytical data for **8**: ^{1}H NMR (300 MHz, methanol-d_4) δ ppm 3.34−3.44 (m, 1H), 3.70−3.92 (m, 3H), 4.12 (dd, J = 8.52, 3.57 Hz, 1H), 4.71−4.80 (m, 1H), 6.08 (d, J = 2.75 Hz, 1H), 7.30−7.41 (m, 1H), 7.41−7.51 (m, 2H), 7.77−7.90 (m, 2H), 8.51 (s, 1H). ^{13}C NMR (100 MHz, methanol-d_4) δ ppm 62.6, 68.7, 70.1, 72.6, 78.7, 88.5, 122.1, 126.8 (×2), 129.5, 130.0 (×2), 131.5, 149.1. MS-ESI found: [M + Na$^+$] 330.2.

4′-[(α-D-Mannopyranosylcarbonyl)amino]-[1,1′-biphenyl]-3-car-boxylic Acid Methyl Ester (11). The solution of 2,3,4,6-tetra-O-acetyl-α-D-mannosyl cyanide (**9**)[29,30] (0.107g, 0.3 mmol) in 25% hydrochloric acid was heated at 50 °C for 48 h. The solvent was removed. Water (10 mL) and H+ exchange resin (DOWEX 50WX4-100) was added and kept stirring for 5 min. The resin was filtered off, and the filtrate was concentrated and then dried in vacuo to give crude α-D-mannopyranosyl carboxylic acid (**10**). To the crude product, 1-[bis(dimethylamino)methylene]-1H-1,2,3-triazolo[4,5-b]pyridinium 3-oxid hexafluorophosphate (HATU) (0.274 g, 0.72 mmol) and anhydrous DMF (6 mL) were added at 0 °C. After stirring for 10 min, methyl 4′-aminobiphenyl-3-carboxylate (0.164 g, 0.72 mmol), and then N,N-diisopropylethylamine (0.233 g, 1.80 mmol) were added. The mixture was stirred overnight while being warmed to rt naturally. The solvent was removed and the residue was purified by silica gel chromatography (methanol−dichloromethane gradient elution) to give the title compound (0.066 g) in 52% yield. Analytical data for **11**: ^{1}H NMR (300 MHz, methanol-d_4) δ ppm 3.50 (dt, J =

4.67, 2.33 Hz, 1H), 3.58−3.65 (m, 2H), 3.76 (dd, J = 11.81, 7.42 Hz, 1H), 3.86−4.03 (m, 4H), 4.52 (t, J = 2.61 Hz, 1H), 4.57 (d, J = 2.75 Hz, 1H), 7.55 (t, J = 7.69 Hz, 1H), 7.60−7.68 (m, 2H), 7.68−7.76 (m, 2H), 7.82−7.91 (m, 1H), 7.97 (dt, J = 7.69, 1.37 Hz, 1H), 8.21−8.28 (m, 1H). ^{13}C NMR (100 MHz, methanol-d_4) δ ppm 52.7, 63.3, 68.5, 70.1, 73.2, 79.6, 80.4, 121.9 (×2), 128.4 (×2), 128.6, 129.1, 130.2, 132.0, 132.4, 137.4, 138.9, 142.2, 168.5, 170.1. ESI-MS found: [M + H$^+$] 418.1.

4-Bromo-N-[(α-D-mannopyranosyl)methyl]-benzamide (13). To a solution of [(α-D-mannopyranosyl)methyl]amine (**12**) (0.58 mmol) (obtained from 2,3,4,6-tetra-O-acetyl-α-D-mannosyl cyanide **9**[29,30]) in pyridine (10 mL) was added 4-bromo-benzoyl chloride (2.2 g, 10 mmol), and the reaction was stirred at RT overnight. Excess acid chloride was quenched by the addition of MeOH (2 mL). After 30 min, the reaction was concentrated in vacuo and dried. To the crude residue was added 25 mL of [0.5 M] sodium methoxide in MeOH (pH ∼ 10), and the reaction was stirred for 3 h at RT. H$^+$ exchange resin (DOWEX 50WX4-100) was washed with MeOH and then added while stirring for 15 min. After filtration, the crude product was obtained by concentrating the filtrate and then was purified by silica gel chromatography (methanol−dichloromethane gradient elution). It was found that pyridine-HCl was a large contaminant, so the crude product was redissolved in MeOH (10 mL) and charged with 0.5 mL of 3 M NaOH and stirred for 5 min. The reaction was then neutralized with H$^+$ exchange resin (DOWEX 50WX4-100). After filtration and concentrating the filtrate, the title product was isolated (120 mg, 0.32 mmol; 55% over 2 steps). Analytical data for **13**: ^{1}H NMR (400 MHz, methanol-d_4) δ ppm 3.63−3.68 (m, 4H), 3.75−3.85 (m, 4H), 4.03−4.07 (m, 1H), 7.63 (d, J = 8.8 Hz, 1H), 7.75 (d, J = 8.4 Hz, 1H). ^{13}C NMR (100 MHz, methanol-d_4) δ ppm 40.2, 62.6, 70.0, 70.3, 72.7, 76.3, 77.4, 127.1, 130.3 (×2), 132.7 (×2), 134.6. ESI-MS found: [M + H$^+$] 376.0 (100%), 378.0 (97.3%).

4′-[[[(α-D-Mannopyranosyl)methyl]amino]carbonyl]-[1,1′biphen-yl]-3-carboxylic Acid Methyl Ester (14). To a stirred solution of 4-bromo-N-[(α-D-mannopyranosyl)methyl]-benzamide (**13**) (0.38 g, 0.1 mmol), 3-methoxycarbonylphenylboronic acid (0.027 g, 0.15 mmol), and cesium carbonate (0.098 g, 0.3 mmol) in dioxane/water (5 mL/1 mL) under nitrogen atmosphere was added tetrakis-(triphenylphosphine)palladium (0.012 g, 0.01 mmol) was heated at 80 °C for 1 h. The reaction was concentrated to dryness and dissolved in DMSO and was purified by HPLC [C18, 15 mm × 150 mm column; eluent, acetonitrile/water (0.1% TFA)]. After lyopholiztion of pure fractions, the title compound (24 mg, 0.056 mmol) was obtained in 55% yield. Analytical data for **14**: ^{1}H NMR (400 MHz, methanol-d_4) δ ppm 3.68−3.71 (m, 4H), 3.78−3.83 (m, 3H), 3.87 (t, J = 3.2 Hz, 1H), 3.93 (s, 3H), 4.07−4.15 (m, 1H), 7.57 (t, J = 7.6 Hz, 1H), 7.73 (d, J = 7.6 Hz, 2H), 7.89 (d, J = 8.0 Hz, 1H), 7.94 (d, J = 8.0 Hz, 2H), 8.01 (dd, J = 1.6, 8.0 Hz, 1H), 8.26 (s, 1H). ^{13}C NMR (100 MHz, methanol-d_4) δ ppm 40.2, 52.8, 62.7, 69.9, 70.4, 72.7, 76.5, 77.5, 128.1 (×2), 129.0, 129.2 (×2), 129.9, 130.4, 132.1, 132.7, 134.8, 141.7, 144.4, 168.3, 170.0. ESI-MS found: [M + H$^+$] 432.2.

2,3,4,6-Tetra-O-benzyl-α-D-mannopyranosyl Cyanide (15). Similar to the synthesis of compound **9**, acetyl 2,3,4,6-tetra-O-benzyl-α-D-mannopyranoside (56.97 g, 97.84 mmol) was dissolved into dry acetonitrile (800 mL) under N$_2$, and the reaction was cooled to 0 °C. Trimethylsilyl cyanide (36.86 mL, 293.53 mmol) was added, followed by the dropwise addition of boron trifluoride diethyl etherate (2.46 mL, 19.57 mmol). After 5 min, the reaction was brought to rt and stirred for an additional 30 min. Upon completion, brine (400 mL) and ethyl acetate (400 mL) were added and the reaction was stirred vigorously for 5 min. The layers were then partitioned, and the aqueous layer was extracted with ethyl acetate (3 × 100 mL). The organic portions were then combined and washed with 1 M aq HCl (2 × 200 mL) and brine (200 mL). The organic layer was dried over Na$_2$SO$_4$ and concentrated in vacuo. The crude residue contained a 2:1 mixture of α- and β-anomers, which were easily separated by silica gel chromatography (ethyl acetate−hexanes gradient), the more nonpolar product being the desired α-mannoside **15**, obtained in 51% yield (the β-mannoside byproduct was obtained in 27% yield). Analytical data for **15**:[31b] ^{1}H NMR (300 MHz, chloroform-d) δ ppm 3.72−3.76 (m, 1H),

3.80−3.91 (m, 3H), 3.93−3.97 (m, 1H), 4.01−4.08 (m, 1H), 4.51−4.71 (m, 7H), 4.81 (d, J = 2.3 Hz, 1H), 4.88 (d, J = 11.0 Hz, 1H), 7.17−7.22 (m, 2H), 7.27−7.40 (m, 18H). ESI-MS found: [M + Na$^+$] 572.2.

2,3,4,6-Tetra-O-benzyl-α-D-mannopyranosyl Carbaldehyde (16). Similarly to previously reported protocols,[31b,39] at −78 °C, DIBAL/hexane (1.0 M, 11.3 mL) was added dropwise into the solution of 2,3,4,6-tetra-*O*-benzyl-α-D-mannopyranosyl cyanide (**15**) (4.97 g, 9.04 mmol) in CH$_2$Cl$_2$ (150 mL) under N$_2$. The mixture was stirred for 30 min, maintaining a temperature of −78 °C. Then, the reaction was diluted with CH$_2$Cl$_2$ (150 mL) and then acidified with the addition of 0.2 M aq HCl (400 mL), stirring for 10 min at rt, and then filtered through Celite (to help break up emulsion) into a separatory funnel. The distinct layers were separated, and the aqueous layer was then extracted an additional time with CH$_2$Cl$_2$. The two organic fractions were combined and washed 2× with brine (100 mL). The organic layer was dried over Na$_2$SO$_4$, which also cleared up any remaining emulsion, and then concentrated to give intermediate carbaldehyde **16** as the crude product. Because of its instability, this intermediate was used without further purification, after drying 30 min to 1 h under high vacuum. Compound **16** was confirmed by ESI-MS, found [M + Na$^+$] 575.5.

(2,3,4,6-Tetra-O-benzyl-α-D-mannopyranosyl)-(4-bromophenyl)-methan-1(R/S)-ol (17R/S). Into a flask containing 1,4-dibromobenzene (0.354 g, 1.5 mmol) in ether (5 mL) was added BuLi/hexanes (2.5 M, 0.5 mL) at −78 °C. One hour later, crude aldehyde **16** (synthesized from 0.56 mmol of carbonitrile **15**) was added. The mixture was stirred at −78 °C for 1 h and then was warmed slowly to −40 °C over 1 h. Then 0.5 N aq HCl was used to quench the reaction, and ethyl acetate was use for extraction. The organic layer was collected, dried with Na$_2$SO$_4$, and concentrated, and the resulting residue was partially purified by silica gel chromatography (ethyl acetate−hexane gradient elution). The diastereomers, (2,3,4,6-tetra-*O*-benzyl-α-D-mannopyranosyl)-(4-bromophenyl)-methan-1(*R*)-ol (**17R**) and (2,3,4,6-tetra-*O*-benzyl-α-D-mannopyranosyl)-(4-bromophenyl)-methan-1(*S*)-ol (**17S**) were separated and collected, the more nonpolar fractions containing intermediate **17R**. After separation, the impure compounds **17R** (0.075 g, 0.1 mmol) and **17S** (0.034 g, 0.048 mmol) were used without further purification in the synthesis of **18R** and **18S**, respectively. Both compounds **17R** and **17S** were separately confirmed by ESI-MS, found [M + Na$^+$] 731.1.

4′-[(2,3,4,6-Tetra-O-benzyl-α-D-mannopyranosyl)-(R)-hydroxy-methyl]-N-methyl-[1,1′biphenyl]-3-carboxamide (18R). Following the general Suzuki-coupling procedure, the impure mannosyl bromide **17R** (0.075 g, 0.1 mmol), commercially available *N*-methyl-3-(4,4,5,5-tetramethyl-[1,3,2]dioxaborolan-2-yl)-benzamide (0.039g, 0.15 mmol), cesium carbonate (0.098 g, 0.3 mmol), and tetrakis-(triphenylphosphine)palladium (0.012 g, 0.01 mmol) in dioxane/water (5 mL/1 mL) were stirred under N$_2$, at 80 °C for 1 h. Upon completion, the solvent was removed, and the resulting residue was purified by silica gel chromatography (methanol−dichloromethane gradient elution) to give 4′-[(2,3,4,6-tetra-*O*-benzyl-α-D-mannopyranosyl)-(*R*)-hydroxymethyl]-*N*-methyl-[1,1′biphenyl]-3-carboxamide (**18R**) in 9% total yield (0.039 g, 0.051 mmol) (3 steps; based on 0.56 mmol carbonitrile **15**). Analytical data for **18R**: ^{1}H NMR (300 MHz, acetonitrile-d_3) δ ppm 2.89 (d, J = 4.7 Hz, 3H), 3.49−3.69 (m, 2H), 3.72−3.83 (m, 2H), 3.85−3.96 (m, 1H), 4.06 (dd, J = 8.0, 3.0 Hz, 2H), 4.13−4.22 (m, 1H), 4.27−4.46 (m, 2H), 4.48−4.68 (m, 5H), 4.76 (d, J = 11.3 Hz, 1H), 4.90−5.00 (m, 1H), 7.03−7.15 (m, 1H), 7.18−7.41 (m, 20H), 7.43−7.56 (m, 3H), 7.57−7.65 (m, 2H), 7.69−7.80 (m, 2H), 8.00 (t, J = 1.6 Hz, 1H). ESI-MS found: [M + Na$^+$] 786.2.

4′-[(2,3,4,6-Tetra-O-benzyl-α-D-mannopyranosyl)-(S)-hydroxy-methyl]-N-methyl-[1,1′biphenyl]-3-carboxamide (18S). The title compound was synthesized from **17S** (0.034 g, 0.048 mmol) following the same procedure described for **18R**. **18S** was obtained in 6.5% (0.028 g, 0.037 mmol) (3 steps, based on 0.56 mmol carbonitrile **15**). Analytical data for **18S**: ^{1}H NMR (300 MHz, acetonitrile-d_3) δ ppm 2.90 (d, J = 4.7 Hz, 3H), 3.48 (d, J = 4.4 Hz, 1H), 3.57−3.62 (m, 1H), 3.62−3.85 (m, 3H), 3.86−3.94 (m, 2H), 3.95−4.03 (m, 1H), 4.33−

4.51 (m, 6H), 4.52−4.76 (m, 2H), 4.85−4.99 (m, 1H), 6.98−7.45 (m, 22H), 7.47−7.68 (m, 4H), 7.71−7.84 (m, 2H), 8.03 (t, J = 1.7 Hz, 1H). ESI-MS found: [M + Na$^+$] 786.2.

(2,3,4,6-Tetra-O-benzyl-α-D-mannopyranosyl)-(4-bromo-2-meth-ylphenyl)-methan-1(R/S)-ol (19R/S). Into a flask containing 4-bromo-2-methyl-iodobenzene (9.04 mL, 63.29 mmol) in anhydrous Et$_2$O (150 mL) under N$_2$ was added BuLi/hexanes (2.5 M, 21.7 mL) dropwise at −78 °C. After 1 h, the freshly prepared crude **16** [from starting material **15** (4.97 g, 9.04 mmol)] was dissolved into Et$_2$O (50 mL) and added via cannula over a period of 5 min. The mixture was stirred at −78 °C for 30 min and then slowly warmed to 0 °C over 1.5 h. Saturated aq NH$_4$Cl was used to quench the reaction, and the reaction was extracted with ethyl acetate (2 × 100 mL). The organic fractions were then combined and washed with brine (100 mL), dried over Na$_2$SO$_4$, and concentrated in vacuo. The resulting residue was mixture of diastereomers, which were purified and separated by silica gel chromatography (1/9, v/v, ethyl acetate−hexanes, isocratic elution) to give (2,3,4,6-tetra-*O*-benzyl-α-D-mannopyranosyl)-(4-bromo-2-methylphenyl)-methan-1(*R*)-ol (**19R**) as a syrup in 16% yield (1.05g, 1.45 mmol) and (2,3,4,6-tetra-*O*-benzyl-α-D-mannopyranosyl)-(4-bromo-2-methylphenyl)-methan-1(*S*)-ol (**19S**) as a syrup in 20% yield (1.30 g, 1.80 mmol); the fractions coming out of the column earlier containing isomer **19R**. Analytical data for **19R**: ^{1}H NMR (400 MHz, chloroform-*d*) δ ppm 2.29 (s, 3H); 3.49 (br s, 1H), 3.70−3.83 (m, 2H), 3.89 (t, J = 5.9 Hz, 1H), 3.94−3.99 (m, 1H), 4.10 (t, J = 5.1 Hz, 1H), 4.13−4.18 (m, 1H), 4.21−4.28 (m, 1H), 4.40 (s, 2H), 4.49 (s, 2H), 4.56−4.64 (m, 3H), 4.71 (d, J = 11.7 Hz, 1H), 5.08 (d, J = 5.1 Hz, 1H), 7.13−7.18 (m, 2H), 7.28−7.41 (m, 21H). ESI-MS found: [M + Na$^+$] 745.5 (100%), 747.5 (97.3%). Analytical data for **19S**: ^{1}H NMR (400 MHz, chloroform-*d*) δ ppm 2.18 (s, 3H), 3.19 (br s, 1H), 3.67−3.73 (m, 2H), 3.76−3.85 (m, 3H), 4.03−4.11 (m, 2H), 4.44−4.62 (m, 7H), 4.67−4.73 (m, 1H), 5.06 (d, J = 5.5 Hz, 1H), 7.16−7.37 (m, 23H). ESI-MS found: [M + Na$^+$] 745.5 (100%), 747.5 (97.3%).

Two-Step Oxidation and Reduction Protocol to Convert 19S into 19R (Step 1 19S to 19a). *(2,3,4,6-Tetra-O-benzyl-α-D-mannopyranosyl)-(4-bromo-2-methylphenyl)-methanone (19a).* The **19S** product was converted into the **19R** isomer via a two-step oxidation reduction procedure. First, oxidation to the ketone intermediate (**19a**) was achieved by dissolving **19S** (0.58 g, 0.80 mmol) in dry CH$_2$Cl$_2$ (50 mL) and dry pyridine (0.16 mL, 2.01 mmol) under N$_2$ at 0 °C. Dess−Martin periodinane (DMP) (0.68 g, 1.61 mmol) was added portionwise, and the reaction mixture was kept at 0 °C for 1 h and then allowed to warm to 15 °C over an additional 1.5 h. Upon completion, the reaction flask was cooled in an ice bath and a 1:1 mixture of 10% aq Na$_2$S$_2$O$_3$ (6 mL) and saturated aq NaHCO$_3$ (6 mL) was added, and the reaction was stirred for 5 min at rt. The layers were then separated, and the aqueous layer was extracted an additional time with CH$_2$Cl$_2$ (5 mL). The organic fractions were combined and washed sequentially with saturated aq NaHCO$_3$ (10 mL) and brine (10 mL), dried over Na$_2$SO$_4$, and concentrated in vacuo without heating. The residue was quickly purified by silica gel chromatography (ethyl acetate−hexane gradient elution), and pure compound eluent was again concentrated in vacuo in the absence of heat to afford the desired ketone intermediate (2,3,4,6-tetra-*O*-benzyl-α-D-mannopyranosyl)-(4-bromo-2-methylphenyl)-methanone (**19a**) in 74% yield (0.43 g, 0.59 mmol). Analytical data for **19a**: ^{1}H NMR (400 MHz, chloroform-*d*) δ ppm 2.40 (s, 3H), 3.50−3.56 (m, 1H), 3.61 (d, J = 10.6 Hz, 1H), 3.67−3.77 (m, 2H), 4.05 (t, J = 9.0 Hz, 1H), 4.43 (d, J = 12.1 Hz, 1H), 4.49−4.61 (m, 3H), 4.64−4.74 (m, 2H), 4.76−4.85 (m, 2H), 4.89 (d, J = 11.0 Hz, 1H), 5.12 (d, J = 2.7 Hz, 1H), 7.19−7.24 (m, 2H), 7.31−7.45 (m, 20H), 7.60 (d, J = 8.6 Hz, 1H). ESI-MS found: [M + Na$^+$] 743.5 (100%), 745.5 (97.3%).

Two-Step Oxidation and Reduction Protocol to Convert 19S into 19R (Step 2 19a to 19R). *(2,3,4,6-Tetra-O-benzyl-α-D-mannopyranosyl)-(4-bromo-2-methylphenyl)-methan-1(R)-ol (19R).* Next, selective reduction to the (*R*)-alcohol was achieved by reacting ketone (**19a**) (0.31 g, 0.43 mmol) in dry THF (30 mL) under N$_2$ at −40 °C, with the dropwise addition of lithium tri-*tert*-butoxyaluminum hydride (1 M in hex; 0.87 mL, 0.87 mmol). The

reaction was warmed to 0 °C over 1 h and then stirred an additional 1 h at 0 °C. Upon completion, the reaction was diluted with ethyl acetate (60 mL). Saturated aq potassium sodium tartrate (30 mL) was added, and the reaction was vigorously stirred 1 h at rt. At this time, the layers were separated and the aqueous layer was additionally extracted with ethyl acetate (2 × 15 mL), using 1 M aq HCl to break up any remaining emulsion. The organic fractions were then combined, dried over Na$_2$SO$_4$, and concentrated in vacuo. The residue was purified by silica gel chromatography (ethyl acetate–hexane gradient elution) to afford the desired *R*-isomer **19R** (0.26 g, 0.36 mmol) in 84% yield (with 16% of the **19S** (0.050 g, 0.069 mmol) isomer also generated). Analytical data as reported above.

4′-[(2,3,4,6-Tetra-O-benzyl-α-D-mannopyranosyl)-(R/S)-hydroxy-methyl]-N,3′-dimethyl-[1,1′biphenyl]-3-carboxamide (20R/S). The title compound was synthesized following the general Suzuki-coupling procedure. Although separable, for this reaction the purified **19R/S** (0.130 g, 0.18 mmol, generated from the reaction of aldehyde **16**) was taken as a mixture of isomers and was reacted with commercially available N-methyl-3-(4,4,5,5-tetramethyl-[1,3,2]dioxaborolan-2-yl)-benzamide (0.071g, 0.27 mmol), cesium carbonate (0.176 g, 0.54 mmol), and tetrakis(triphenylphosphine)palladium (0.021 g, 0.018 mmol) in dioxane/water (5 mL/1 mL), and the reaction was stirred under N$_2$, at 80 °C for 1 h. Upon completion, the solvent was removed and the resulting products were separated and purified by silica gel chromatography (methanol–dichloromethane gradient elution). **20R** (0.046 g, 0.059 mmol) was obtained in 33% yield as the more nonpolar compound, and the more polar **20S** (0.055 g, 0.071 mmol) was obtained in 39% yield. Analytical data for **20R**: ¹H NMR (400 MHz, chloroform-*d*) δ ppm 2.38 (s, 3H), 2.88–3.17 (m, 4H), 3.65 (dd, *J* = 10.6, 4.3 Hz, 1H), 3.71–3.84 (m, 2H), 4.02 (d, *J* = 5.5 Hz, 2H), 4.09–4.21 (m, 2H), 4.30–4.44 (m, 4H), 4.51–4.68 (m, 4H), 5.17 (dd, *J* = 5.9, 3.1 Hz, 1H), 6.15 (d, *J* = 4.7 Hz, 1H), 7.08–7.39 (m, 22H), 7.43–7.54 (m, 2H), 7.62–7.67 (m, 1H), 7.68–7.73 (m, 1H), 7.87–7.90 (m, 1H). MS (ESI) found: [M + Na⁺] 800.6. Analytical data for **20S**: ¹H NMR (400 MHz, chloroform-*d*) δ ppm 2.27 (s, 3H), 3.03 (d, *J* = 4.8 Hz, 3H), 3.13 (br s, 1H), 3.61–3.89 (m, 5H), 3.98–4.10 (m, 1H), 4.12–4.20 (m, 1H), 4.33–4.61 (m, 7H), 4.69 (d, *J* = 11.4 Hz, 1H), 5.14 (d, *J* = 5.1 Hz, 1H), 6.19 (d, *J* = 4.3 Hz, 1H), 7.04–7.59 (m, 24H), 7.61–7.76 (m, 2H), 7.91–8.01 (m, 1H). ESI-MS found: [M + Na⁺] 800.6.

4′-[(α-D-Mannopyranosyl)-(R)-hydroxymethyl]-N,3′-dimethyl-[1,1′biphenyl]-3-carboxamide (21R). Compound **20R** (0.046 g, 0.059 mmol) and 10% wt Pd/C (0.050 g, 0.024 mmol) were stirred in MeOH (5 mL) under 1 atm of H$_2$ for 16 h. The Pd/C was then filtered off, and the filtrate was concentrated in vacuo. The resulting residue was purified by HPLC [C18, 15 mm × 150 mm column; eluent, acetonitrile/water (0.05% TFA)] to give **21R** (0.020 g, 0.048 mmol) in 81% yield. [Compound **22** was also isolated as a product in 12% yield (0.003 g, 0.0072 mmol)]. ¹H NMR (400 MHz, methanol-*d*$_4$) δ ppm 2.51 (s, 3H), 2.95 (s, 3H), 3.57–3.78 (m, 4H), 4.00–4.07 (m, 1H), 4.10 (dd, *J* = 6.9, 2.4 Hz, 1H), 4.25 (t, *J* = 2.9 Hz, 1H), 5.24 (d, *J* = 6.7 Hz, 1H), 7.45–7.57 (m, 3H), 7.62 (d, *J* = 8.2 Hz, 1H), 7.71–7.83 (m, 2H), 8.07 (t, *J* = 1.6 Hz, 1H). ¹³C NMR (100 MHz, methanol-*d*$_4$) δ ppm 19.6, 26.9, 63.0, 69.0, 69.9, 71.0, 73.3, 78.2, 81.6, 125.6, 126.7, 126.9, 128.9, 130.1, 130.1, 130.9, 136.1, 137.7, 140.5, 141.2, 142.6, 170.7. ESI-MS found: [M + Na⁺] 440.3.

4′-[(α-D-Mannopyranosyl)-(S)-hydroxymethyl]-N,3′-dimethyl-[1,1′biphenyl]-3-carboxamide (21S). The title compound was synthesized from **20S** (0.055 g, 0.071 mmol), following the same procedure as for **21R**. Compound **21S** (0.025 g, 0.062 mmol) was obtained in 88% yield. Analytical data for **21S**: ¹H NMR (400 MHz, methanol-*d*$_4$) δ ppm 2.51 (s, 3H), 2.95 (s, 3H), 3.56 (dd, *J* = 1.0 Hz, 1H), 3.67 (d, *J* = 8.2 Hz, 1H), 3.70–3.82 (m, 3H), 3.91 (d, *J* = 9.4 Hz, 1H), 4.10 (dd, *J* = 9.0, 2.0 Hz, 1H), 5.28 (d, *J* = 8.6 Hz, 1H), 7.34–7.63 (m, 4H), 7.69–7.90 (m, 2H), 8.07 (s, 1H). ¹³C NMR (100 MHz, methanol-*d*$_4$) δ ppm 19.9, 27.0, 63.4, 67.5, 69.0, 69.9, 73.6, 77.3, 83.4, 126.0, 126.7, 127.0, 129.2, 130.1, 130.3, 130.9, 136.1, 137.4, 140.2, 140.9, 142.3, 170.6. ESI-MS found: [M + Na⁺] 440.3.

4′-[(α-D-Mannopyranosyl)methyl]-N,3′-dimethyl-[1,1′biphenyl]-3-carboxamide (22). The title compound was obtained from the preparation of **21R** as a side-product in 12% yield (0.003 g, 0.0072 mmol). Analytical data for **22**: ¹H NMR (400 MHz, methanol-*d*$_4$) δ ppm 2.44 (s, 3H), 2.95 (s, 3H), 3.04 (d, *J* = 7.4 Hz, 2H), 3.69 (m, 3H), 3.83 (m, 2H), 3.86–3.92 (m, 1H), 4.04–4.21 (m, 1H), 7.31 (d, *J* = 7.8 Hz, 1H), 7.42–7.47 (m, 1H), 7.50 (m, 2H), 7.75 (m, 2H), 8.05 (s, 1H). ¹³C NMR (100 MHz, methanol-*d*$_4$) δ ppm 19.8, 26.9, 33.7, 63.1, 69.3, 72.1, 72.7, 76.5, 79.4, 125.6, 126.6, 126.8, 130.0, 130.1, 130.9, 131.7, 136.1, 137.8, 138.1, 139.8, 142.7, 170.7. ESI-MS found: [M + H⁺] 402.3.

4′-(2,3,4,6-Tetra-O-acetyl-α-D-mannopyranosyloxy)-N,3′-dimeth-yl-[1,1′biphenyl]-3-carboxamide (23a). 4′-(-α-D-Mannopyranosy-loxy)-N,3′-dimethyl-[1,1′biphenyl]-3-carboxamide[20b] (0.072 g, 0.178 mmol) was dissolved in anhydrous pyridine (1 mL) and acetic anhydride (1 mL). The solvent was removed in vacuo, and the residue was purified by HPLC [C18, 15 mm × 150 mm column; eluent, acetonitrile/water (0.1% TFA)]. Pure fractions were combined and lyophilized to give the title compound as a white powder in 62% yield (0.063 g, 0.11 mmol). Analytical data for **23a**: ¹H NMR (400 MHz, dimethyl sulfoxide-*d*$_6$) δ ppm 1.94 (s, 3H), 2.00 (s, 3H), 2.05 (s, 3H), 2.16 (s, 3H), 2.32 (s, 3H), 2.81 (d, *J* = 4.30 Hz, 3H), 3.93–4.11 (m, 2H), 4.19 (dd, *J* = 12.13, 5.09 Hz, 1H), 5.22 (t, *J* = 9.98 Hz, 1H), 5.33–5.45 (m, 2H), 5.80 (s, 1H), 7.23 (d, *J* = 8.61 Hz, 1H), 7.46–7.65 (m, 3H), 7.77 (d, *J* = 7.83 Hz, 2H), 8.07 (s, 1H), 8.54 (d, *J* = 4.30 Hz, 1H). ¹³C NMR (100 MHz, chloroform-*d*) δ ppm 16.4, 20.8 (×3), 21.0, 27.0, 62.3, 66.0, 69.2, 69.5, 69.6, 96.0, 114.7, 125.3, 125.7, 125.7, 128.1, 129.0, 129.7, 130.0, 135.0, 135.3, 141.1, 153.9, 168.4, 169.9, 170.1, 170.2, 170.7. ESI-MS found: [M + Na⁺] 594.3.

4′-(6-Dihydrogen Phosphate-α-D-mannopyranosyloxy)-N,3′-di-methyl-[1,1′biphenyl]-3-carboxamide (23b). 4′-(-α-D-Mannopyrano-syloxy)-N,3′-dimethyl-[1,1′biphenyl]-3-carboxamide[20b] (0.20 g, 0.5 mmol) was dissolved in trimethyl phosphate (5 mL) and water (9 uL, 0.5 mmol). The reaction was cooled to 0 °C, and then phosphoryl trichloride (142 μL, 1.5 mmol) was slowly added and then stirred for 3 h at 0 °C. The reaction was neutralized by adding crushed ice and then conc ammonia. The solvent was removed in vacuo, and the residue was purified by HPLC [C18, 15 mm × 150 mm column; eluent, acetonitrile/water (0.1% TFA)]. Pure fractions were combined and lyophilized to give the title compound as a white powder in 29% yield (0.070 g, 0.145 mmol). Analytical data for **23b**: ¹H NMR (400 MHz, dimethyl sulfoxide-*d*$_6$) δ ppm 2.26 (s, 3H), 2.81 (d, *J* = 4.70 Hz, 3H), 3.42–3.68 (m, 3H), 3.75 (dd, *J* = 9.00, 3.13 Hz, 1H), 3.86–3.97 (m, 2H), 4.03 (dd, *J* = 9.78, 5.87 Hz, 1H), 5.45 (d, *J* = 1.96 Hz, 1H), 7.24 (d, *J* = 8.61 Hz, 1H), 7.43–7.60 (m, 3H), 7.76 (dd, *J* = 7.43, 1.57 Hz, 2H), 8.06 (s, 1H), 8.56 (d, *J* = 4.30 Hz, 1H). ¹³C NMR (100 MHz, dimethyl sulfoxide-*d*$_6$) δ ppm 16.1, 26.3, 66.3, 70.1, 70.6, 73.3, 73.3, 98.7, 115.1, 124.8, 125.4, 125.6, 127.3, 128.8, 128.9, 129.1, 133.0, 135.1, 139.9, 154.3, 166.6. ESI-MS found: [M + H⁺] 484.3

4′-[6-O-(N,N-Dimethylaminoacetyl)-α-D-mannopyranosyloxy]-N,3′-dimethyl-[1,1′biphenyl]-3-carboxamide (23c). Step 1: 4′-(-α-D-Mannopyranosyloxy)-N,3′-dimethyl-[1,1′biphenyl]-3-carboxamide[20b] (0.202 g, 0.50 mmol) was stirred in a flask with triethylamine (0.38 mL, 2.75 mmol) and anhydrous DMF (2 mL) at under N$_2$ at 0 °C. Trimethylsilyl chloride (0.35 mL, 2.75 mmol) was added dropwise, and the reaction was brought to rt and stirred an additional 3.5 h. The reaction was then quenched with ice water, and the reaction mixture was extracted twice with ethyl acetate. The organic extractions were then combined and concentrated under reduced pressure to give the crude 4′-[2,3,4,6-tetra-O-trimethylsilyl-α-D-mannopyranosyloxy]-N,3′-dimethyl-[1,1′biphenyl]-3-carboxamide intermediate, which was then redissolved in acetone/methanol (1/1.5 mL). The reaction was cooled to 0 °C, and acetic acid (0.055 mL, 0.96 mmol) was added. The reaction was allowed to slowly warm to rt and was monitored for progress by TLC (ethyl acetate–hexanes, 1/1). After 9 h, NaHCO$_3$ (0.16 g, 1.90 mmol) was added and the solvents were removed in vacuo. Purification by silica gel chromatography (ethyl acetate–hexanes gradient elution) gave the corresponding 4′-[2,3,4,-tri-O-trimethylsilyl-α-D-mannopyranosyloxy]-N,3′-dimethyl-[1,1′biphenyl]-3-carboxamide in 61% yield (0.19 g, 0.36 mmol). Analytical data: ¹H NMR (400 MHz, chloroform-*d*) δ ppm 0.18 (d, *J* = 4.3 Hz, 18H), 0.23 (s, 9H), 1.90 (dd, *J* = 7.0, 5.9 Hz, 1H), 2.30 (s, 3H), 3.05 (d, *J* = 4.7

Hz, 3H), 3.62−3.68 (m, 1H), 3.69−3.77 (m, 2H), 4.01−4.05 (m, 3H), 5.39 (d, J = 1.6 Hz, 1H), 6.20 (br s, 1H), 7.17 (d, J = 8.6 Hz, 1H), 7.36−7.44 (m, 2H), 7.45−7.50 (m, 1H), 7.67 (dt, J = 7.7, 1.8 Hz, 2H), 7.95 (t, J = 1.8 Hz, 1H). ESI-MS found: [M + H⁺] 489.4;

Step 2: N,N-Dimethylglycine hydrochloride (0.0154 g, 0.11 mmol) was dissolved into CH₂Cl₂/diisopropylethylamine (DIPEA) (5/0.2 mL). Dimethylaminopyridine (DMAP) (0.0024 g, 0.02 mmol) was added, followed by the 4′-[2,3,4,-tri-O-trimethylsilyl-α-D-mannopyr-anosyloxy]-N,3′-dimethyl-[1,1′biphenyl]-3-carboxamide (0.062 g, 0.10 mmol) from step 1 and finally N,N-diisopropylcarbodiimide (DIC) (0.020 mL, 0.13 mmol). The reaction was stirred for 16 h and then solvent was removed under reduced pressure and the residue was redissolved into acetonitrile (3 mL) and the reaction was cooled to 0 °C. Trifluoroacetic acid (0.08 mL) was added, and the reaction was stirred for 2 h at 0 °C. The solvent was removed in vacuo, and the residue was purified by HPLC [C18, 15 mm × 150 mm column; eluent, acetonitrile/water (0.1% TFA)]. Pure fractions were combined and lyophilized to give the title compound as a white powder (0.015 g, 0.031 mmol) in 31% yield. Analytical data for 23c: ¹H NMR (400 MHz, methanol-d₄) δ ppm 2.32 (s, 3H), 2.89 (s, 6H), 2.95 (s, 3H), 3.71−3.85 (m, 2H), 3.94−4.00 (m, 1H), 4.06 (d, J = 5.48 Hz, 2H), 4.11 (t, J = 2.54 Hz, 1H), 4.42 (m, 1H), 4.61 (dd, J = 11.74, 1.56 Hz, 1H), 5.57 (d, J = 1.57 Hz, 1H), 7.23 (d, J = 8.61 Hz, 1H), 7.47−7.53 (m, 3H), 7.73−7.78 (m, 2H), 8.05 (m, 1H). ¹³C NMR (100 MHz, methanol-d₄) δ ppm 16.5, 27.0, 44.4 (×2), 57.9, 66.5, 68.3, 71.9, 72.5, 72.8, 99.9, 115.6, 126.4, 126.5, 126.5, 129.0, 130.1, 130.6, 130.6, 135.3, 136.1, 142.3, 155.5, 166.7, 170.7. ESI-MS found: [M + H⁺] 489.4;

(2,3,4,6-Tetra-O-benzyl-α-D-mannopyranosyl)-(4-bromo-2-meth-ylphenyl)-methan-1(R)-ol Acetate (26). Dimethylaminopyridine (8.9 mg, 0.07 mmol) and (2,3,4,6-tetra-O-benzyl-α-D-mannopyranosyl)-(4-bromo-2-methylphenyl)-methan-1(R)-ol (19R) (1.06 g, 1.47 mmol) were dissolved in dry pyridine (5 mL) under N₂, and the reaction was cooled to 0 °C. Acetic anhydride (0.21 mL, 2.21 mmol) was added dropwise, and after 5 min the ice bath was removed. After stirring 1 h at rt, the reaction was cooled to 0 °C and quenched with MeOH (0.5 mL) and the pyridine was removed in vacuo. The residue was redissolved in CH₂Cl₂, (25 mL) and washed successively with water (10 mL), 1 M aq HCl (2 × 10 mL), and water (10 mL), dried over Na₂SO₄, and concentrated in vacuo. The residue was purified by silica gel chromatography (ethyl acetate−hexane gradient elution) to afford compound 26 (1.11 g, 1.46 mmol) in 99% yield. Analytical data for 26: ¹H NMR (400 MHz, chloroform-d) δ ppm 1.91 (s, 3H), 2.38 (s, 3H), 3.60−3.69 (m, 1H), 3.69−3.78 (m, 1H), 3.78−3.87 (m, 2H), 3.91−4.04 (m, 2H), 4.34 (dd, J = 6.7, 3.5 Hz, 1H), 4.39−4.46 (m, 1H), 4.50−4.69 (m, 6H), 4.81 (d, J = 11.3 Hz, 1H), 6.15 (d, J = 6.7 Hz, 1H), 7.07−7.13 (m, 1H), 7.23−7.38 (m, 22H). ESI-MS found: [M + Na⁺] 787.5 (100%), 789.5 (97.3%).

(2,3,4,6-Tetra-O-acetyl-α-D-mannopyranosyl)-(4-bromo-2-meth-ylphenyl)-methan-1(R)-ol Acetate (27). Following a modified literature protocol for benzyl ether removal,[40] (2,3,4,6-tetra-O-benzyl-α-D-mannopyranosyl)-(4-bromo-2-methylphenyl)-methan-1(R)-ol acetate (26) (1.0 g, 1.30 mmol) was dissolved in dry CH₂Cl₂ (50 mL) under N₂, and the reaction was cooled to −78 °C. Boron trichloride (1 M in CH₂Cl₂; 10.4 mL, 10.4 mmol) was added dropwise, and the reaction was stirred for 30 min. Once removal of the benzyl ethers was complete, the excess reagent was quenched by the addition of MeOH (1 mL). At this time, it was observed (via TLC and LCMS) that upon quenching, a minor product corresponding to benzylic acetate cleavage was produced. The reaction mixture containing both the tetraacetate and pentaacetate intermediates was concentrated under reduced pressure and purified by silica gel chromatography (methanol−dichloromethane gradient elution). Both intermediates were collected and combined and then redissolved in dry pyridine (10 mL) under N₂, and the reaction was cooled to 0 °C. Dimethylaminopyridine (7.0 mg, 0.06 mmol) was added, followed by acetic anhydride (0.77 mL, 8.16 mmol), and the reaction was stirred for 5 min at 0 °C, then brought to rt. After 1 h, the reaction was cooled to 0 °C and quenched with MeOH (0.25 mL). The pyridine was removed in vacuo, and the residue was then redissolved in CH₂Cl₂, (25 mL) and washed successively with water (10 mL), 1 M aq HCl (2

× 10 mL), and water (10 mL), dried over Na₂SO₄, and concentrated in vacuo. Purification by silica gel chromatography (ethyl acetate−hexanes gradient) gave the desired compound 27 (0.51 g, 0.88 mmol) in 68% yield. Analytical data for 27: mp 115−118 °C (diethyl ether−hexanes). ¹H NMR (400 MHz, chloroform-d) δ ppm 1.90 (s, 3H), 1.97 (s, 3H), 2.01 (s, 6H), 2.08 (s, 3H), 2.37 (s, 3H), 3.84−3.90 (m, 1H), 3.94 (dd, J = 12.1, 2.0 Hz, 1H), 4.14−4.23 (m, 2H), 5.10 (t, J = 8.6 Hz, 1H), 5.30 (dd, J = 9.0, 3.1 Hz, 1H), 5.47 (t, J = 2.9 Hz, 1H), 6.12 (d, J = 7.0 Hz, 1H), 7.15−7.20 (m, 1H), 7.23−7.30 (m, 2H). ESI-MS found: [M + Na⁺] 595.2 (100%), 597.2 (97.3%).

7-(4-[(α-D-Mannopyranosyl)-(R)-hydroxymethyl]-3-methylphen-yl]-1(2H)-isoquinolinone (28R). Following the general Suzuki-coupling procedure, the acetylated mannosyl bromide 27 (0.10 g, 0.174 mmol), commercially available1-hydroxyisoquinoline-7-boronate ester (0.095 g, 0.35 mmol), cesium carbonate (0.17 g, 0.052 mmol), and tetrakis(triphenylphosphine)palladium (0.03 g, 0.026 mmol) in dioxane/water (5 mL/1 mL) were reacted under N₂ at 80 °C for 1.5 h. Upon completion, the reaction was then cooled to rt, and solvents were evaporated under reduced pressure. The crude reaction residue was then redissolved into CH₂Cl₂ (typically a colorless solid byproduct remains insoluble) and partially purified by column chromatography to remove metal catalysts and salts to give the impure acetate-protected intermediate. The mannoside intermediate was then redissolved in MeOH (3 mL) and cooled to 0 °C. [1 M] Sodium methoxide in MeOH was added dropwise until a pH of 9−10 was achieved. After 5 min, the ice bath was removed and the reaction was stirred for 2 h. Upon completion, the reaction was neutralized with H⁺ exchange resin (DOWEX 50WX4-100). The resin was filtered, and the filtrate was concentrated in vacuo. The resulting residue was purified by HPLC [(C18, 15 mm × 150 mm column; eluent, acetonitrile/water (0.05% TFA)] to give compound 28R (0.035 g, 0.082 mmol) in 47% yield. Analytical data for 28R: ¹H NMR (400 MHz, methanol-d₄) δ ppm 2.52 (s, 3H), 3.64−3.75 (m, 4H), 4.05 (br s, 1H), 4.09−4.15 (m, 1H), 4.26 (br s, 1H), 5.25 (d, J = 6.7 Hz, 1H), 6.70 (d, J = 7.0 Hz, 1H), 7.18 (d, J = 7.0 Hz, 1H), 7.52−7.61 (m, 2H), 7.62−7.67 (m, 1H), 7.72 (d, J = 8.2 Hz, 1H), 8.00 (d, J = 8.6 Hz, 1H), 8.54 (s, 1H). ¹³C NMR (100 MHz, methanol-d₄) δ ppm 19.6, 63.0, 69.0, 69.9, 71.0, 73.2, 78.3, 81.6, 107.7, 125.5, 125.5, 127.3, 128.2, 128.8, 129.0, 130.0, 132.6, 137.8, 138.8, 140.1, 140.7, 141.3, 165.1. ESI-MS found: [M + H⁺] 428.4, [M − 18 + H⁺] 410.3, [2M + H⁺] 855.6.

3,4-Dihydro-7-(4-[(α-D-mannopyranosyl)-(R)-hydroxymethyl]-3-methylphenyl]-1(2H)-isoquinolinone (29R). Following the general Suzuki-coupling procedure, mannosyl bromide 19R (0.220 g, 0.304 mmol), commercially available1-hydroxyisoquinoline-7-boronate ester (0.165 g, 0.608 mmol), cesium carbonate (0.297 g, 0.912 mmol), and tetrakis(triphenylphosphine)palladium (0.046 g, 0.053 mmol) in dioxane/water (10 mL/2 mL) were reacted under N₂, at 80 °C for 1.5 h. Upon completion, the reaction was then cooled to rt and solvents were evaporated under reduced pressure. The crude reaction residue was then redissolved into CH₂Cl₂ (typically a colorless solid byproduct remains insoluble) and partially purified by column chromatography to remove metal catalysts and salts to give the impure benzyl-protected intermediate. The mannoside intermediate was then redissolved in MeOH (5 mL), and 10% wt Pd/C (0.150 g, 0.14 mmol) was added. The reaction was stirred under 1 atm of H₂ for 16 h. Upon completion, the Pd/C was filtered off and the filtrate was concentrated and dried in vacuo. The resulting residue was purified by HPLC [(C18, 15 mm × 150 mm column; eluent, acetonitrile/water (0.05% TFA)] to give compound 29R (0.06 mg, 0.140 mmol) in 46% yield. Analytical data for 29R: ¹H NMR (400 MHz, methanol-d₄) δ ppm 2.49 (s, 3H), 3.01 (t, J = 6.7 Hz, 2H), 3.52 (t, J = 6.7 Hz, 2H), 3.63−3.74 (m, 4H), 4.05 (br s, 1H), 4.10 (dd, J = 6.7, 2.0 Hz, 1H), 4.25 (t, J = 2.5 Hz, 1H), 5.24 (d, J = 7.0 Hz, 1H), 7.37 (d, J = 7.8 Hz, 1H), 7.44−7.53 (m, 2H), 7.61 (d, J = 7.8 Hz, 1H), 7.75 (dd, J = 7.8, 2.0 Hz, 1H), 8.18 (d, J = 1.6 Hz, 1H). ¹³C NMR (100 MHz, methanol-d₄) δ ppm 19.6, 28.7, 40.8, 63.0, 69.0, 69.9, 71.0, 73.2, 78.2, 81.6, 125.3, 126.6, 128.9, 129.2, 129.8, 130.2, 131.7, 137.6, 139.7, 140.2, 141.0, 141.1, 168.3. ESI-MS found: [M + H⁺] 430.4, [M − 18 + H⁺] 412.4, [2M + H⁺] 859.6.

3,4-Dihydro-7-[4-(α-D-mannopyranosyloxy)-3-methylphenyl]-1(2H)-isoquinolinone (30). The previously reported compound 7-[4-(α-D-mannopyranosyloxy)-3-methylphenyl]-isoquinolin-1-one[20b] (25) (30 mg, 0.073 mmol) was dissolved into MeOH (3 mL), and 10% wt Pd/C (30 mg) was added. The reaction was stirred under 1 atm of H_2 for 16 h, after which the reaction was filtered and the filtrate was concentrated in vacuo. The resulting residue was purified by HPLC [(C18, 15 mm × 150 mm column; eluent, acetonitrile/water (0.05% TFA)] to give compound 30 (0.30 mg, 0.072 mmol) in 99% yield. Analytical data for 30: ^{1}H NMR (400 MHz, methanol-d_4) δ ppm 2.30 (s, 3H), 2.96−3.03 (m, 2H), 3.49−3.55 (m, 2H), 3.57−3.65 (m, 1H), 3.72−3.81 (m, 3H), 3.97 (d, J = 9.4 Hz, 1H), 4.08 (br s, 1H), 5.55 (s, 1H), 7.31 (dd, J = 19.4, 8.0 Hz, 2H), 7.40−7.47 (m, 2H), 7.70 (d, J = 7.8 Hz, 1H), 8.14 (s, 1H). ^{13}C NMR (100 MHz, methanol-d_4) δ ppm 16.6, 28.7, 40.9, 62.7, 68.4, 72.1, 72.7, 75.5, 99.9, 115.9, 126.3, 126.3, 128.9, 129.1, 130.2, 131.5, 135.1, 139.2, 141.0, 155.7, 168.4. ESI-MS found: [M + H$^+$] 416.4, [2M + H$^+$] 831.6.

7-(4,4,5,5-Tetramethyl-1,3,2-dioxaborolan-2-yl)isoquinolin-1-amine (31a) and Isoquinolin-1-amine-7 Boronic Acid (31b). Potassium acetate (264 mg, 2.69 mmol) was activated by adding it to a round-bottom flask, which was then heated to 250 °C under vacuum for 2 min and then allowed to cool to rt under vacuum for an additional 10 min, after which time a nitrogen atmosphere was continuously maintained. Dry DMSO (2 mL) was added, followed by the addition of commercially available 7-bromoisoquinolin-1-amine (150 mg, 0.67 mmol) and bis(pinacolato)diboron (256 mg, 1.0 mmol). Pd(dppf)Cl$_2$ (49.2 mg, 0.067 mmol) was added, and the reaction flask was evacuated under high vacuum and then backfilled with N$_2$ three times. The flask was then placed in an oil bath preheated to 80 °C and allowed to stir for 2.5 h. The reaction was cooled to rt, and solvents were evaporated under reduced pressure. The crude reaction residue was then redissolved into CH$_2$Cl$_2$ and allowed to sit for 5 min to allow for byproducts to precipitate. The precipitate was filtered off. Evaporation of the CH$_2$Cl$_2$ in vacuo resulted in more byproduct precipitation, and so the residue was redissolved in CH$_2$Cl$_2$ and the process was repeated until no further precipitation was observed. The crude brown residue was then diluted with water (1 mL) and lyophilized to removed trace DMSO, resulting in a brown solid, which was comosed of a mix of the boronate ester and the boronic acid (31a/b), as determined by LCMS. This crude mixture was used without further purification. Analytical data for 31a: ESI-MS found, [M + H$^+$] 271.3. Analytical data for 31b: ESI-MS found, [M + H$^+$] 189.2

7-(4-[(α-D-Mannopyranosyl)-(R)-hydroxymethyl]-3-methylphenyl)-isoquinolin-1-amine (31R). Following the general Suzuki-coupling procedure, mannosyl bromide 27 (0.092 g, 0.160 mmol), isoquinolin-1-amine-7-boronate ester/acid 31a/b (0.086, 0.32 mmol), cesium carbonate (0.16 g, 0.48 mmol), and tetrakis(triphenylphosphine)-palladium (0.028 g, 0.024 mmol) in dioxane/water (5 mL/1 mL) were reacted under N$_2$ at 80 °C for 1.5 h. Upon completion, the solvent was removed under reduced pressure and mixture was filtered through a silica gel column (ethyl acetate−hexanes, 2/1 isocratic elution) to remove the metal catalyst and salts. The filtrate was concentrated then dried in vacuo. The crude compound was then redissolved into MeOH (3 mL) and cooled to 0 °C. Sodium methoxide [1M] in MeOH was added dropwise until a pH of 9−10 was achieved. After 5 min, the ice bath was removed and the reaction was stirred for 30 min. Upon completion, the reaction was neutralized with H$^+$ exchange resin (DOWEX 50WX4-100). The resin was filtered, and the filtrate was concentrated in vacuo. The resulting residue was purified by HPLC [(C18, 15 mm × 150 mm column; eluent, acetonitrile/water (0.05% TFA)] to give compound 31R (0.018 g, 0.042 mmol) in 26% yield. Analytical data for 31R: ^{1}H NMR (400 MHz, methanol-d_4) δ ppm 8.71 (s, 1H), 8.26 (d, J = 8.2 Hz, 1H), 7.97 (d, J = 8.6 Hz, 1H), 7.62−7.72 (m, 3H), 7.54 (d, J = 7.0 Hz, 1H), 7.24 (d, J = 7.0 Hz, 1H), 5.27 (d, J = 7.0 Hz, 1H), 4.27 (t, J = 2.9 Hz, 1H), 4.13 (dd, J = 6.8, 2.2 Hz, 1H), 4.01−4.07 (m, 1H), 3.63−3.73 (m, 4H), 2.55 (s, 3H). ^{13}C NMR (100 MHz, methanol-d_4) δ ppm 19.7, 63.0, 69.0, 69.9, 70.8, 73.1, 78.4, 81.5, 113.0, 119.6, 123.6, 125.8, 127.8, 129.3, 129.6, 130.3, 135.0,

137.7, 138.1, 138.9, 142.3, 143.0, 156.1. ESI-MS found: [M + H$^+$] 427.4.

5-(4-[(α-D-Mannopyranosyl)-(R)-hydroxymethyl]-3-methylphenyl)-isoquinoline (32R). Following the general Suzuki-coupling procedure, mannosyl bromide 27 (0.092 g, 0.160 mmol), commercially purchased 5-isoquinolinylboronic acid (0.056 g, 0.32 mmol), cesium carbonate (0.16 g, 0.48 mmol), and tetrakis(triphenylphosphine)palladium (0.028 g, 0.024 mmol) in dioxane/water (5 mL/1 mL) were reacted under N$_2$ at 80 °C for 1.5 h. Upon completion, the solvent was removed under reduced pressure and mixture was filtered through a silica gel column (ethyl acetate−hexanes, 2/1 isocratic elution) to remove the metal catalyst and salts. The filtrate was concentrated then dried in vacuo. The crude compound was then redissolved into MeOH (5 mL) and cooled to 0 °C. Sodium methoxide [1M] in MeOH was added dropwise until a pH of 9−10 was achieved. After 5 min, the ice bath was removed and the reaction was stirred for 30 min. Upon completion, the reaction was neutralized with H$^+$ exchange resin (DOWEX 50WX4-100). The resin was filtered, and the filtrate was concentrated in vacuo. The resulting residue was purified by HPLC [(C18, 15 mm × 150 mm column; eluent, acetonitrile/water (0.05% TFA)] to give compound 32R (0.025 g, 0.060 mmol) in 38% yield. Analytical data for 32R: ^{1}H NMR (400 MHz, methanol-d_4) δ ppm 9.75 (s, 1H), 8.48 (dd, J = 15.8, 7.2 Hz, 2H), 8.28 (d, J = 6.7 Hz, 1H), 8.02−8.13 (m, 2H), 7.74 (d, J = 7.8 Hz, 1H), 7.37 (d, J = 8.6 Hz, 1H), 7.34 (s, 1H), 5.30 (d, J = 7.0 Hz, 1H), 4.28 (br s, 1H), 4.14−4.19 (m, 1H), 4.04 (br s, 1H), 3.69 (br s, 4H), 2.54 (s, 3H). ^{13}C NMR (100 MHz, methanol-d_4) δ ppm 19.6, 63.1, 69.1, 70.1, 70.8, 73.2, 78.4, 81.4, 124.2, 128.5, 129.1, 129.6, 129.6, 130.7, 131.5, 132.9, 134.2, 137.4, 137.6, 138.1, 141.6, 142.3, 149.6. ESI-MS found: [M + H$^+$] 412.3.

7-[4-(α-D-Mannopyranosyloxy)-3-methylphenyl]- isoquinolin-1-amine (33). Step 1: Under nitrogen atmosphere, the mixture of 4-bromo-2-methylphenyl 2,3,4,6-tetra-O-acetyl-α-D-mannopyranoside[20b] (2.869 g, 5.55 mmol), bis(pinacolato)diboron (1.690g, 6.66 mmol), potassium acetate (2.177 g, 22.18 mmol), and (1.1′-bis-(diphenylphosohino)ferrocene)dichloropalladium(II) (Pd(dppf)Cl$_2$) (0.244 g, 0.33 mmol) in DMSO (50 mL) was heated at 80 °C with stirring for 2 h. The solvent was removed, and the resulting residue was purified by silica gel chromatography (ethyl acetate−dichloromethane gradient elution) to give the intermediate boronate ester, 2-methyl-4-[4,4,5,5-tetramethyl-(1,3,2)dioxaborolan-2-yl]phenyl 2,3,4,6-tetra-O-acetyl-α-D-mannopyranoside (33a),[25] (2.50 g, 4.43 mmol) in 79% yield. Analytical data: ^{1}H NMR (400 MHz, chloroform-d) δ ppm 1.34 (s, 12H), 2.05 (d, J = 2.3 Hz, 6H), 2.06 (s, 3H), 2.21 (s, 3H), 2.30 (s, 3H), 4.03−4.09 (m, 2H), 4.27−4.33 (m, 1H), 5.39 (t, J = 12.0 Hz, 1H), 5.48 (dd, J = 3.3, 1.8 Hz, 1H), 5.54−5.60 (m, 2H), 7.09 (d, J = 8.2 Hz, 1H), 7.55−7.67 (m, 2H). ESI-MS found: [M + Na$^+$] 587.4.

Step 2: Following the general Suzuki-coupling procedure, 33a (0.150, 0.27 mmol) from step 1, 7-bromoisoquinolin-1-amine (0.060, 0.27 mmol), cesium carbonate (0.26 g, 0.80 mmol), and tetrakis(triphenylphosphine)palladium (0.031 g, 0.027 mmol) in dioxane/water (5 mL/1 mL) were reacted under N$_2$, at 80 °C for 1.5 h. Upon completion, the solvent was removed under reduced pressure, and mixture was filtered through a silica gel column (ethyl acetate−hexanes, 2/1 isocratic elution) to remove the metal catalyst and salts. The filtrate was concentrated then dried in vacuo. The crude compound was then redissolved into MeOH (3 mL) and cooled to 0 °C. Sodium methoxide [1M] in MeOH was added dropwise until a pH of 9−10 was achieved. After 5 min, the ice bath was removed and the reaction was stirred for 2 h. Upon completion, the reaction was neutralized with H$^+$ exchange resin (DOWEX 50WX4-100). The resin was filtered, and the filtrate was concentrated in vacuo. The resulting residue was purified by HPLC [(C18, 15 mm × 150 mm column; eluent, acetonitrile/water (0.05% TFA)] to give compound 33 (0.040 g, 0.097 mmol) in 36% yield. Analytical data for 33: ^{1}H NMR (400 MHz, methanol-d_4) δ ppm 2.34 (s, 3H), 3.57−3.64 (m, 1H), 3.72−3.83 (m, 3H), 3.98 (dd, J = 9.4, 3.1 Hz, 1H), 4.10 (br s, 1H), 5.60 (s, 1H), 7.21 (d, J = 6.7 Hz, 1H), 7.36 (d, J = 8.2 Hz, 1H), 7.52 (d, J = 7.0 Hz, 1H), 7.59 (d, J = 8.6 Hz, 1H), 7.64 (s, 1H), 7.93 (d, J = 8.6 Hz, 1H), 8.21 (d, J = 8.6 Hz, 1H), 8.64 (s, 1H). ^{13}C NMR (100 MHz,

methanol-d_4) δ ppm 16.6, 62.7, 68.4, 72.1, 72.7, 75.6, 99.8, 113.0, 116.0, 119.6, 123.0, 127.0, 127.6, 129.2, 129.5, 130.6, 133.6, 134.8, 137.3, 142.9, 156.0, 156.4. ESI-MS found: [M + H$^+$] 413.4.

Hemagglutination Assay. The hemagglutination inhibition (HAI) assay was performed with UTI89 bacteria and guinea pig red blood cells, as previously described.[25]

Biofilm Assay. The biofilm assay was performed with UTI89 bacteria as previously described.[25]

Differential Scanning Fluorimetry (DSF). The DSF assay was performed with FimH$_L$ (10 μM) in the absence or presence of 100 μM mannoside, as previously described.[25]

Computational Molecular Modeling. Computer-generated docking was performed with AutoDock Vina. Ligand coordinates were generated in eLBOW within the Phenix program suite. Simple optimization of mannosides **21R** and **21S**, as described by its SMILES sequence, was manually inspected and modified to ensure the correct chair conformation of the mannose pucker. These pdb coordinates were then converted to pdbqt format using Babel. The X-ray coordinates of FimH from the **23** co-crystal structure was converted to its topology file using AutoDock Tools. The grid box was centered at the mannose binding pocket of FimH, and its dimensions (40 × 40 × 40 Å^3) were chosen to accommodate multiple potential binding modes at or near the binding pocket. The exhaustiveness of the search was set to a value of 20. The top binding modes and scores within this grid space were generated by AutoDock Vina and visualized in PyMOL.

Animal Infections. The bacterial inoculum and infection of mice was performed as previously described.[20a] Briefly, the bacterial strain UTI89 with a kanamycin antibiotic cassette inserted in the chromosome (UTI89$_{KAN}$) was grown under type 1-inducing conditions, 2 × 24 static growth in LB at 37 °C. Bacteria were harvested, washed, and resuspended in sterile PBS to the appropriate concentration. Six to eight week C3H/HeN female mice were purchased from Envigo (formerly Harlan Laboratories). Mice were anesthetized by inhalation of isoflurane and infected by transurethral inoculation of 50 μL of bacterial suspension at the appropriate density. At the designated time point, mice were killed by cervical dislocation under anesthesia and bladders harvested and processed by mechanical disruption. Processed bladders were serially diluted and plated on LB with 50 μg/mL of kanamycin to enumerate bacterial burden.

Treatment of Chronic Urinary Tract Infection in Mice. Mice were infected with 1–2 × 10^8 UTI89$_{KAN}$, and the infection was allowed to continue for 2 weeks. Twelve days post inoculation, the urine from mice was collected and titered to identify chronically infected mice (urine titers ≥10^5). At 2 weeks post inoculation, chronically infected mice were treated orally with 100 μL of mannoside resuspended in 10% cyclodextrin to the appropriate concentration to generate the designated dosage. Bladders were harvested and titered to determine the bacterial burden at the designated time points following treatment.

Prophylactic Treatment of Acute Urinary Tract Infection in Mice. Prophylactic treatment of mice involved oral delivery of mannoside at 25 mg/kg 30 min prior to infection with UTI89$_{KAN}$. Mice were infected with 1–2 × 10^7 UTI89$_{KAN}$, and bladders were harvested and titered to determine the bacterial burden 6 h following inoculation.

Mouse Pharmacokinetic (PK) Studies. For dosing in mice, 100 μL of a solution of mannoside in 10% cyclodextrin [10 mg/mL (50 mg/kg)] was inoculated with a gavage needle into the mouse stomach. Urine was collected at 1, 3, 6, and 8 h after dosing and spiked with an internal standard. Analysis for test article levels by LC–MS/MS was performed using a C18 reversed phase column and an AB Sciex API-4000 QTrap instrument (a gradient of acetonitrile and water in 0.1% formic acid), with ion spray detection (+) ESI. Selected reaction monitoring (SRM) mode quantification was performed for the following MS/MS transitions [precursor mass/charge ratio (m/z)/ product m/z]: compound **21R**, 418.20/238.20 amu; compound **23**, 404.20/242.20 amu (Levels of **23** were quantitated after dosing of prodrug, **23a**); compound **24**, 461.20/299.20 amu.

ASSOCIATED CONTENT

Ⓢ Supporting Information

The Supporting Information is available free of charge on the ACS Publications website at DOI: 10.1021/acs.jmedchem.6b00948.

> ^{1}H and ^{13}C NMR, HPLC, and MS analytical data for new compounds and the details of the crystallography experiments, including the X-ray crystal determinants for both for the small molecule **27** and FimH co-crystal structure with **23**; details of the prophylactic acute UTI mouse model with **23** and prodrugs **23a**–**c**, as well as the rat pharmacokinetic study of **21R**, **23**, and **25** (PDF)
> Molecular formula strings (CSV)

AUTHOR INFORMATION

Corresponding Author

*Phone: 314-362-0509. Fax: 314-362-7183. E-mail: janetkaj@biochem.wustl.edu. Address: 660 South Euclid Avenue, Box 8231, St. Louis, Missouri 63110, United States.

Author Contributions

#L.M.-M. and Z.C. contributed equally to the work

Notes

The authors declare the following competing financial interest(s): Scott Hultgren and James Janetka are co-founders and stockholders in Fimbrion Therapeutics, Inc.

ABBREVIATIONS USED

UTI, urinary tract infection; UPEC, uropathogenic *E. coli*; CFUs, colony forming units; SAR, structure–activity relationships; SPR, structure–property relationships; HA, hemagglutination; HAI, hemagglutination Inhibition; IBC, intracellular bacterial community; PD, pharmacodynamics; PK, pharmacokinetics; C_{max}, concentration maximum

REFERENCES

(1) (a) Boyle, E. C.; Finlay, B. B. Bacterial pathogenesis: exploiting cellular adherence. *Curr. Opin. Cell Biol.* **2003**, *15*, 633–639. (b) Chagnot, C.; Listrat, A.; Astruc, T.; Desvaux, M. Bacterial adhesion to animal tissues: protein determinants for recognition of extracellular matrix components. *Cell. Microbiol.* **2012**, *14*, 1687–1696.

(2) (a) Ofek, I.; Beachey, E. H. General concepts and principles of bacterial adherence. In *Bacterial Adherence, Receptors and Recognition*, Beachey, E. H., Ed.; Chapman and Hall: London, 1980; Vol. 6, pp 1–29. (b) Ofek, I.; Doyle, R. J. Common Themes in Bacterial Adhesion. In *Bacterial Adhesion to Cells and Tissues*; Chapman and Hall: New York, 1994; pp 513–561.

(3) Aminov, R. I. A brief history of the antibiotic era: lessons learned and challenges for the future. *Front. Microbiol.* **2010**, *1*, 134.

(4) (a) Cole, S. T. Who will develop new antibacterial agents? *Philos. Trans. R. Soc., B* **2014**, *369*, 20130430. (b) Walsh, C. Where will new antibiotics come from? *Nat. Rev. Microbiol.* **2003**, *1*, 65−70.

(5) (a) Lee, Y. M.; Almqvist, F.; Hultgren, S. J. Targeting virulence for antimicrobial chemotherapy. *Curr. Opin. Pharmacol.* **2003**, *3*, 513−519. (b) Rasko, D. A.; Sperandio, V. Anti-virulence strategies to combat bacteria-mediated disease. *Nat. Rev. Drug Discovery* **2010**, *9*, 117−128.

(6) (a) Ofek, I.; Hasty, D. L.; Sharon, N. Anti-adhesion therapy of bacterial diseases: prospects and problems. *FEMS Immunol. Med. Microbiol.* **2003**, *38*, 181−191. (b) Cozens, D.; Read, R. C. Anti-adhesion methods as novel therapeutics for bacterial infections. *Expert Rev. Anti-Infect. Ther.* **2012**, *10*, 1457−1468. (c) Bouckaert, J.; Berglund, J.; Schembri, M.; De Genst, E.; Cools, L.; Wuhrer, M.; Hung, C. S.; Pinkner, J.; Slattegard, R.; Zavialov, A.; Choudhury, D.; Langermann, S.; Hultgren, S. J.; Wyns, L.; Klemm, P.; Oscarson, S.; Knight, S. D.; De Greve, H. Receptor binding studies disclose a novel class of high-affinity inhibitors of the Escherichia coli FimH adhesin. *Mol. Microbiol.* **2005**, *55*, 441−455.

(7) Jones, C. H.; Pinkner, J. S.; Roth, R.; Heuser, J.; Nicholes, A. V.; Abraham, S. N.; Hultgren, S. J. FimH adhesin of type 1 pili is assembled into a fibrillar tip structure in the Enterobacteriaceae. *Proc. Natl. Acad. Sci. U. S. A.* **1995**, *92*, 2081−2085.

(8) Hung, C. S.; Bouckaert, J.; Hung, D.; Pinkner, J.; Widberg, C.; DeFusco, A.; Auguste, C. G.; Strouse, R.; Langermann, S.; Waksman, G.; Hultgren, S. J. Structural basis of tropism of Escherichia coli to the bladder during urinary tract infection. *Mol. Microbiol.* **2002**, *44*, 903−915.

(9) Puorger, C.; Vetsch, M.; Wider, G.; Glockshuber, R. Structure, folding and stability of FimA, the main structural subunit of type 1 pili from uropathogenic Escherichia coli strains. *J. Mol. Biol.* **2011**, *412*, 520−535.

(10) Zhou, G.; Mo, W. J.; Sebbel, P.; Min, G.; Neubert, T. A.; Glockshuber, R.; Wu, X. R.; Sun, T. T.; Kong, X. P. Uroplakin Ia is the urothelial receptor for uropathogenic Escherichia coli: evidence from in vitro FimH binding. *J. Cell Sci.* **2001**, *114*, 4095−4103.

(11) Eto, D. S.; Jones, T. A.; Sundsbak, J. L.; Mulvey, M. A. Integrin-mediated host cell invasion by type 1-piliated uropathogenic Escherichia coli. *PLoS Pathog.* **2007**, *3*, e100.

(12) Anderson, G. G.; Palermo, J. J.; Schilling, J. D.; Roth, R.; Heuser, J.; Hultgren, S. J. Intracellular bacterial biofilm-like pods in urinary tract infections. *Science* **2003**, *301*, 105−107.

(13) Griebling, T. L. Urinary tract infection in women. In *Urologic Diseases in America*; Litwin, M.S., Saigal, C.S., Eds.; U.S. Government Printing Office: Washington, DC, 2007; pp 587−620.

(14) (a) Foxman, B. Epidemiology of urinary tract infections: incidence, morbidity, and economic costs. *DM, Dis.-Mon.* **2003**, *49*, 53−70. (b) Kärkkäinen, U. M.; Ikäheimo, R.; Katila, M. L.; Siitonen, A. Recurrence of urinary tract infections in adult patients with community- acquired pyelonephritis caused by E. coli: a 1-year follow-up. *Scand. J. Infect. Dis.* **2000**, *32*, 495−499. (c) Ikähelmo, R.; Siitonen, A.; Heiskanen, T.; Kärkkäinen, U.; Kuosmanen, P.; Lipponen, P.; Mäkelä, P. H. Recurrence of urinary tract infection in a primary care setting: analysis of a 1-year follow-up of 179 women. *Clin. Infect. Dis.* **1996**, *22*, 91−99. (d) Foxman, B. Urinary tract infection syndromes: occurrence, recurrence, bacteriology, risk factors, and disease burden. *Infect. Dis. Clin. North Am.* **2014**, *28*, 1−13.

(15) Ronald, A. R.; Nicolle, L. E.; Stamm, E.; Krieger, J.; Warren, J.; Schaeffer, A.; Naber, K. G.; Hooton, T. M.; Johnson, J.; Chambers, S.; Andriole, V. Urinary tract infection in adults: research priorities and strategies. *Int. J. Antimicrob. Agents* **2001**, *17*, 343−348.

(16) (a) Karlowsky, J. A.; Hoban, D. J.; Decorby, M. R.; Laing, N. M.; Zhanel, G. G. Fluoroquinolone-resistant urinary isolates of Escherichia coli from outpatients are frequently multidrug resistant: results from the North American Urinary Tract Infection Collaborative Alliance-Quinolone Resistance study. *Antimicrob. Agents Chemother.* **2006**, *50*,

2251−2254. (b) *National Disease and Therapeutic Index*; IMS Health, Inc.: Plymouth Meeting, PA, 2004.

(17) Blango, M. G.; Mulvey, M. A. Persistence of uropathogenic Escherichia coli in the face of multiple antibiotics. *Antimicrob. Agents Chemother.* **2010**, *54*, 1855−1863.

(18) Mydock-McGrane, L. K.; Cusumano, Z. T.; Janetka, J. W. Mannose-derived FimH antagonists: a promising anti-virulence therapeutic strategy for urinary tract infections and Crohn's disease. *Expert Opin. Ther. Pat.* **2016**, *26*, 175−197.

(19) (a) Martinez-Medina, M.; Garcia-Gil, L. J. Escherichia coli in chronic inflammatory bowel diseases: An update on adherent invasive Escherichia coli pathogenicity. *World J. Gastrointest. Pathophysiol.* **2014**, *5*, 213−227. (b) Boudeau, J.; Barnich, N.; Darfeuille-Michaud, A. Type 1 pili-mediated adherence of Escherichia coli strain LF82 isolated from Crohn's disease is involved in bacterial invasion of intestinal epithelial cells. *Mol. Microbiol.* **2001**, *39*, 1272−1284.

(20) (a) Cusumano, C. K.; Pinkner, J. S.; Han, Z.; Greene, S. E.; Ford, B. A.; Crowley, J. R.; Henderson, J. P.; Janetka, J. W.; Hultgren, S. J. Treatment and prevention of urinary tract infection with orally active FimH inhibitors. *Sci. Transl. Med.* **2011**, *3*, 109ra115. (b) Han, Z.; Pinkner, J. S.; Ford, B.; Chorell, E.; Crowley, J. M.; Cusumano, C. K.; Campbell, S.; Henderson, J. P.; Hultgren, S. J.; Janetka, J. W. Lead optimization studies on FimH antagonists: discovery of potent and orally bioavailable ortho-substituted biphenyl mannosides. *J. Med. Chem.* **2012**, *55*, 3945−3959. (c) Han, Z.; Pinkner, J. S.; Ford, B.; Obermann, R.; Nolan, W.; Wildman, S. A.; Hobbs, D.; Ellenberger, T.; Cusumano, C. K.; Hultgren, S. J.; Janetka, J. W. Structure-based drug design and optimization of mannoside bacterial FimH antagonists. *J. Med. Chem.* **2010**, *53*, 4779−4792.

(21) (a) Firon, N.; Ashkenazi, S.; Mirelman, D.; Ofek, I.; Sharon, N. Aromatic alpha-glycosides of mannose are powerful inhibitors of the adherence of type 1 fimbriated Escherichia coli to yeast and intestinal epithelial cells. *Infect. Immun.* **1987**, *55*, 472−476. (b) Firon, N.; Ofek, I.; Sharon, N. Carbohydrate-binding sites of the mannose-specific fimbrial lectins of Enterobacteria. *Infect. Immun.* **1984**, *43*, 1088−1090. (c) Firon, N.; Ofek, I.; Sharon, N. Interaction of mannose-containing oligosaccharides with the fimbrial lectin of Eshcerichia coli. *Biochem. Biophys. Res. Commun.* **1982**, *105*, 1426−1432.

(22) Klein, T.; Abgottspon, D.; Wittwer, M.; Rabbani, S.; Herold, J.; Jiang, X.; Kleeb, S.; Lüthi, C.; Scharenberg, M.; Bezençon, J.; Gubler, E.; Pang, L.; Smiesko, M.; Cutting, B.; Schwardt, O.; Ernst, B. FimH antagonists for the oral treatment of urinary tract infections: from design and synthesis to in vitro and in vivo evaluation. *J. Med. Chem.* **2010**, *53*, 8627−8641.

(23) (a) Kleeb, S.; Pang, L.; Mayer, K.; Eris, D.; Sigl, A.; Preston, R. C.; Zihlmann, P.; Sharpe, T.; Jakob, R. P.; Abgottspon, D.; Hutter, A. S.; Scharenberg, M.; Jiang, X.; Navarra, G.; Rabbani, S.; Smiesko, M.; Ludin, N.; Bezencon, J.; Schwardt, O.; Maier, T.; Ernst, B. FimH antagonists: bioisosteres to improve the in vitro and in vivo PK/PD profile. *J. Med. Chem.* **2015**, *58*, 2221−2239. (b) Sperling, O.; Fuchs, A.; Lindhorst, T. K. Evaluation of the carbohydrate recognition domain of the bacterial adhesin FimH: design, synthesis and binding properties of mannoside ligands. *Org. Biomol. Chem.* **2006**, *4*, 3913−3922. (c) Chalopin, T.; Alvarez Dorta, D.; Sivignon, A.; Caudan, M.; Dumych, T. I.; Bilyy, R. O.; Deniaud, D.; Barnich, N.; Bouckaert, J.; Gouin, S. G. Second generation of thiazolylmannosides, FimH antagonists for E. coli-induced Crohn's disease. *Org. Biomol. Chem.* **2016**, *14*, 3913−3925. (d) Alvarez Dorta, D.; Sivignon, A.; Chalopin, T.; Dumych, T. I.; Roos, G.; Bilyy, R. O.; Deniaud, D.; Krammer, E.-M.; de Ruyck, J.; Lensink, M. F.; Bouckaert, J.; Barnich, N.; Gouin, S. G. The Antiadhesive Strategy in Crohn's Disease: Orally Active Mannosides to Decolonize Pathogenic Escherichia coli from the Gut. *ChemBioChem* **2016**, *17*, 936−952. (e) Brument, S.; Sivignon, A.; Dumych, T. I.; Moreau, N.; Roos, G.; Guerardel, Y.; Chalopin, T.; Deniaud, D.; Bilyy, R. O.; Darfeuille-Michaud, A.; Bouckaert, J.; Gouin, S. G. Thiazolylaminomannosides as potent antiadhesives of type 1 piliated Escherichia coli isolated from Crohn's disease patients. *J. Med. Chem.* **2013**, *56*, 5395−5406. (f) Pang, L.; Kleeb, S.; Lemme, K.; Rabbani, S.; Scharenberg, M.; Zalewski, A.; Schadler, F.; Schwardt, O.;

Ernst, B. FimH antagonists: structure-activity and structure-property relationships for biphenyl alpha-D-mannopyranosides. *ChemMedChem* **2012**, *7*, 1404−1422. (g) Jiang, X.; Abgottspon, D.; Kleeb, S.; Rabbani, S.; Scharenberg, M.; Wittwer, M.; Haug, M.; Schwardt, O.; Ernst, B. Antiadhesion therapy for urinary tract infections—A balanced PK/PD profile proved to be key for success. *J. Med. Chem.* **2012**, *55*, 4700−4713.

(24) (a) Bouckaert, J.; Li, Z.; Xavier, C.; Almant, M.; Caveliers, V.; Lahoutte, T.; Weeks, S. D.; Kovensky, J.; Gouin, S. G. Heptyl alpha-D-mannosides grafted on a beta-cyclodextrin core to interfere with *Escherichia coli* adhesion: an in vivo multivalent effect. *Chem. - Eur. J.* **2013**, *19*, 7847−7855. (b) Gouin, S. G.; Wellens, A.; Bouckaert, J.; Kovensky, J. Synthetic Multimeric Heptyl Mannosides as Potent Antiadhesives of Uropathogenic *Escherichia coli*. *ChemMedChem* **2009**, *4*, 749−755. (c) Touaibia, M.; Wellens, A.; Shiao, T. C.; Wang, Q.; Sirois, S.; Bouckaert, J.; Roy, R. Mannosylated G(0) dendrimers with nanomolar affinities to *Escherichia coli* FimH. *ChemMedChem* **2007**, *2*, 1190−1201. (d) Lindhorst, T. K.; Kieburg, C.; Krallmann-Wenzel, U. Inhibition of the type 1 fimbriae-mediated adhesion of *Escherichia coli* to erythrocytes by multiantennary alpha-mannosyl clusters: the effect of multivalency. *Glycoconjugate J.* **1998**, *15*, 605−613.

(25) Jarvis, C.; Han, Z.; Kalas, V.; Klein, R.; Pinkner, J. S.; Ford, B.; Binkley, J.; Cusumano, C. K.; Cusumano, Z.; Mydock-McGrane, L.; Hultgren, S. J.; Janetka, J. W. Antivirulence Isoquinolone Mannosides: Optimization of the Biaryl Aglycone for FimH Lectin Binding Affinity and Efficacy in the Treatment of Chronic UTI. *ChemMedChem* **2016**, *11*, 367−373.

(26) Vicente, V.; Martin, J.; Jimenez-Barbero, J.; Chiara, J. L.; Vicent, C. Hydrogen-bonding cooperativity: using an intramolecular hydrogen bond to design a carbohydrate derivative with a cooperative hydrogen-bond donor centre. *Chem. - Eur. J.* **2004**, *10*, 4240−4251.

(27) Janetka, J. W.; Han, Z.; Hultgren, S.; Pinkner, J. S.; Cusumano, C. K. Compounds and methods for treating bacterial infections. WO/2011/050323, 2010.

(28) Schwardt, O.; Rabbani, S.; Hartmann, M.; Abgottspon, D.; Wittwer, M.; Kleeb, S.; Zalewski, A.; Smiesko, M.; Cutting, B.; Ernst, B. Design, synthesis and biological evaluation of mannosyl triazoles as FimH antagonists. *Bioorg. Med. Chem.* **2011**, *19*, 6454−6473.

(29) Myers, R. W.; Lee, Y. C. Improved preparations of some per-O-acetylated aldohexopyranosyl cyanides. *Carbohydr. Res.* **1986**, *154*, 145−163.

(30) Maity, S. K.; Dutta, S. K.; Banerjee, A. K.; Achari, B.; Singh, M. Design and Synthesis of Mannose Analogs as Inhibitors of Alpha-Mannosidase. *Tetrahedron* **1994**, *50*, 6965−6974.

(31) (a) Kleeb, S.; Jiang, X.; Frei, P.; Sigl, A.; Bezencon, J.; Bamberger, K.; Schwardt, O.; Ernst, B. FimH Antagonists: Phosphate Prodrugs Improve Oral Bioavailability. *J. Med. Chem.* **2016**, *59*, 3163−3182. (b) Janetka, J. W.; Han, Z.; Hultgren, S.; Pinkner, J. S.; Cusumano, C. K. Compounds and methods for treating bacterial infections. WO/2014/194270, 2014.

(32) Fiege, B.; Rabbani, S.; Preston, R. C.; Jakob, R. P.; Zihlmann, P.; Schwardt, O.; Jiang, X.; Maier, T.; Ernst, B. The tyrosine gate of the bacterial lectin FimH: a conformational analysis by NMR spectroscopy and X-ray crystallography. *ChemBioChem* **2015**, *16*, 1235−1246.

(33) de Ruyck, J.; Lensink, M. F.; Bouckaert, J. Structures of C-mannosylated anti-adhesives bound to the type 1 fimbrial FimH adhesin. *IUCrJ* **2016**, *3*, 163−167.

(34) Tiwari, G.; Tiwari, R.; Rai, A. K. Cyclodextrins in delivery systems: Applications. *J. Pharm. BioAllied Sci.* **2010**, *2*, 72−79.

(35) (a) Elisia, I.; Nakamura, H.; Lam, V.; Hofs, E.; Cederberg, R.; Cait, J.; Hughes, M. R.; Lee, L.; Jia, W.; Adomat, H. H.; Guns, E. S.; McNagny, K. M.; Samudio, I.; Krystal, G. DMSO Represses Inflammatory Cytokine Production from Human Blood Cells and Reduces Autoimmune Arthritis. *PLoS One* **2016**, *11*, e0152538. (b) Grover, S.; Srivastava, A.; Lee, R.; Tewari, A. K.; Te, A. E. Role of inflammation in bladder function and interstitial cystitis. *Ther. Adv. Urol.* **2011**, *3*, 19−33.

(36) (a) Hung, C. S.; Dodson, K. W.; Hultgren, S. J. A murine model of urinary tract infection. *Nat. Protoc.* **2009**, *4*, 1230−1243.

(b) Schwartz, D. J.; Conover, M. S.; Hannan, T. J.; Hultgren, S. J. Uropathogenic *Escherichia coli* superinfection enhances the severity of mouse bladder infection. *PLoS Pathog.* **2015**, *11*, e1004599. (c) Hannan, T. J.; Mysorekar, I. U.; Hung, C. S.; Isaacson-Schmid, M. L.; Hultgren, S. J. Early severe inflammatory responses to uropathogenic *E. coli* predispose to chronic and recurrent urinary tract infection. *PLoS Pathog.* **2010**, *6*, e1001042.

(37) (a) Rosen, D. A.; Hooton, T. M.; Stamm, W. E.; Humphrey, P. A.; Hultgren, S. J. Detection of intracellular bacterial communities in human urinary tract infection. *PLoS Med.* **2007**, *4*, e329. (b) Schlager, T. A.; LeGallo, R.; Innes, D.; Hendley, J. O.; Peters, C. A. B cell infiltration and lymphonodular hyperplasia in bladder submucosa of patients with persistent bacteriuria and recurrent urinary tract infections. *J. Urol.* **2011**, *186*, 2359−2364. (c) Hansson, S.; Hanson, E.; Hjalmas, K.; Hultengren, M.; Jodal, U.; Olling, S.; Svanborg-Eden, C. Follicular cystitis in girls with untreated asymptomatic or covert bacteriuria. *J. Urol.* **1990**, *143*, 330−332. (d) Hannan, T. J.; Roberts, P. L.; Riehl, T. E.; van der Post, S.; Binkley, J. M.; Schwartz, D. J.; Miyoshi, H.; Mack, M.; Schwendener, R. A.; Hooton, T. M.; Stappenbeck, T. S.; Hansson, G. C.; Stenson, W. F.; Colonna, M.; Stapleton, A. E.; Hultgren, S. J. Inhibition of Cyclooxygenase-2 Prevents Chronic and Recurrent Cystitis. *EBioMedicine.* **2014**, *1*, 46−57.

(38) (a) Sattin, S.; Bernardi, A. Glycoconjugates and Glycomimetics as Microbial Anti-Adhesives. *Trends Biotechnol.* **2016**, *34*, 483−495. (b) Cecioni, S.; Imberty, A.; Vidal, S. Glycomimetics versus multivalent glycoconjugates for the design of high affinity lectin ligands. *Chem. Rev.* **2015**, *115*, 525−561. (c) Sutkeviciute, I.; Thepaut, M.; Sattin, S.; Berzi, A.; McGeagh, J.; Grudinin, S.; Weiser, J.; Le Roy, A.; Reina, J. J.; Rojo, J.; Clerici, M.; Bernardi, A.; Ebel, C.; Fieschi, F. Unique DC-SIGN clustering activity of a small glycomimetic: A lesson for ligand design. *ACS Chem. Biol.* **2014**, *9*, 1377−1385. (d) Thepaut, M.; Guzzi, C.; Sutkeviciute, I.; Sattin, S.; Ribeiro-Viana, R.; Varga, N.; Chabrol, E.; Rojo, J.; Bernardi, A.; Angulo, J.; Nieto, P. M.; Fieschi, F. Structure of a glycomimetic ligand in the carbohydrate recognition domain of C-type lectin DC-SIGN. Structural requirements for selectivity and ligand design. *J. Am. Chem. Soc.* **2013**, *135*, 2518−2529. (e) Hauck, D.; Joachim, I.; Frommeyer, B.; Varrot, A.; Philipp, B.; Möller, H. M.; Imberty, A.; Exner, T. E.; Titz, A. Discovery of two classes of potent glycomimetic inhibitors of Pseudomonas aeruginosa LecB with distinct binding modes. *ACS Chem. Biol.* **2013**, *8*, 1775−1784. (f) Chabre, Y. M.; Giguere, D.; Blanchard, B.; Rodrigue, J.; Rocheleau, S.; Neault, M.; Rauthu, S.; Papadopoulos, A.; Arnold, A. A.; Imberty, A.; Roy, R. Combining glycomimetic and multivalent strategies toward designing potent bacterial lectin inhibitors. *Chem. - Eur. J.* **2011**, *17*, 6545−6562. (g) Magnani, J. L.; Ernst, B. Glycomimetic drugs—a new source of therapeutic opportunities. *Discovery Med.* **2009**, *8*, 247−252. (h) Ernst, B.; Magnani, J. L. From carbohydrate leads to glycomimetic drugs. *Nat. Rev. Drug Discovery* **2009**, *8*, 661−677.

(39) Sipos, S.; Jablonkai, I. Preparation of 1-C-glycosyl aldehydes by reductive hydrolysis. *Carbohydr. Res.* **2011**, *346*, 1503−1510.

(40) Lin, C. K.; Cheng, L. W.; Li, H. Y.; Yun, W. Y.; Cheng, W. C. Synthesis of novel polyhydroxylated pyrrolidine-triazole/-isoxazole hybrid molecules. *Org. Biomol. Chem.* **2015**, *13*, 2100−2107.